STUDYING THE FINITENESS OF LARGE EARTHQUAKES WITH HIGHER ORDER MOMENTS OF THE MOMENT TENSOR

by

Rıdvan Örsvuran

B.S., Geophysical Engineering, Istanbul University, 2013

Submitted to Kandilli Observatory and Earthquake
Research Institute in partial fulfillment of the
requirements for the degree of
Master of Science

Graduate Program in Geophysics

Boğaziçi University

2016

STUDYING THE FINITENESS OF LARGE EARTHQUAKES WITH HIGHER ORDER MOMENTS OF THE MOMENT TENSOR

APPROVED BY:

Asst. Prof. Dr. Ali Özgün Konca .....
(Thesis Supervisor)

Asst. Prof. Dr. Çağrı Diner .....
(Thesis Co-supervisor)

Prof. Dr. Mustafa Aktar .....

Prof. Dr. Semih Ergintav .....

Prof. Dr. Argun H. Kocaoğlu .....

DATE OF APPROVAL: 31.05.2016

ACKNOWLEDGEMENTS

I would first like to thank my advisors Assistant Prof. Dr. Ali Özgün Konca and Assistant Prof. Dr. Çağrı Diner. They have guided me during this thesis and created the environment for me to explore on my own. I would also like to thank Prof. Dr. Mustafa Aktar for his valuable inputs.

I would also like to thank Sezim Ezgi Işık, especially for her assistance in the fault modeling process and I would like to acknowledge Ekrem Bekin and Deniz Ertuncay for their valuable comments during this thesis.

Finally, I would like to express my gratitude to my family. I am indebted to them for all of my accomplishments including this one. I would like to thank them for their invaluable support.

ABSTRACT

STUDYING THE FINITENESS OF LARGE EARTHQUAKES WITH HIGHER ORDER MOMENTS OF THE MOMENT TENSOR

Finite fault parameters of the large earthquakes can be obtained using kinematic finite fault models which consist of a collection of subfaults. Yet calculating each subfault individually costs time and the fault model needs to be defined a priori for the inversion process. Alternative representation of the source is defining it as a moment tensor density distribution. In this case higher order moments of the distribution can be calculated. Higher order moments can also be used to estimate first order finite-fault parameters and it has the advantage of having less number of unknowns. This characteristic would allow for more rapid fault parameter solutions. The aim of this thesis is to develop a measure on the approximation of finite fault models using higher order moments up to degree two. Synthetic seismograms for both finite fault sources and their higher order moment approximations are generated using infinite homogeneous isotropic medium to identify the similarities between the waveforms. The effects of the receiver azimuths and distances are investigated using using different frequency ranges. It is found that higher order moments can give an approximation of waveform broadness or pulse width rather than the overall shape of the waveforms. Higher order moments also improved the point source approximations at frequencies that are beyond the corner frequency of the event. Fault type, fault strike direction and receiver azimuth influence the higher order moment solutions while distance is an insignificant factor at least for the whole-space medium which is considered in this study.

ÖZET

BÜYÜK DEPREMLERİN SONLULUĞUNUN YÜKSEK DERECELİ MOMENTLER İLE İNCELENMESİ

Kinematik sonlu fay modelleri kullanılarak büyük depremlerin fay parametreleri bulunabilir. Bu fay modelleri bir çok faycığın bir araya gelmesi ile oluşturulur. Bu modellemenin bir kötü yanı faycıkların etkilerinin tek tek hesaplanmasının zaman alması ve fay modelinin ters işlem için önceden belirlenmesinin zorunlu olmasıdır. Alternatif olarak kaynak moment tensör dağılımı olarak tanımlanabilir. Bu dağılımın yüksek dereceli momentleri de hesaplanabilir. Yüksek dereceli momentler de fay parametrelerinin hesaplanmasında kullanılabilir ve ters işlem için daha az bilinmeyen barındırırlar. Bu özellik ters işlemin daha hızlı yapılmasını sağlar. Bu tezin amacı sonlu fay modellerinin (ikinci dereceye kadar) yüksek dereceli momentler ile ne kadar temsil edilebildiğinin bir ölçüsünü bulmaktır. İzotropik sonsuz homojen ortamda hem sonlu fay yöntemi ile hem de yüksek dereceli momentler ile sentetik sismogram oluşturulup aralarındaki benzerlikler incelenmiştir. Alıcı azimutları ve uzaklıklarının etkileri farklı frekans bantlarında araştırılmıştır. Yüksek dereceli momentlerin dalga şeklinden çok daha genel olarak dalga genişliğine uyum sağladığı görülmüştür. Ayrıca, depremlerin nokta kaynak gibi davranması beklenen frekanslarda yüksek dereceli momentlerin saf nokta kaynak çözümlerine göre sonlu faylara daha iyi uyum sağladığı gözlenmiştir. Sonsuz ortam için uzaklığın çözümlere bir etkisi olmadığı görülmüştür. Ancak, fay tipi, fay atım yönü ve alıcı azimutlarının yüksek dereceli momentlerin çözüm gücüne etkileri belirlenmiştir.

TABLE OF CONTENTS

LIST OF FIGURES

LIST OF SYMBOLS

C_{ijkl}	Elasticity tensor
D	Area or union of areas
e_i	i-th eigenvalue of a matrix
f_i	Body force along i direction
G_{ni}	Green's function
$G_{nk,l}$	Moment tensor Green's function
$H_{nk,l}$	Integral of moment tensor Green's function
$\mathbf{K_T}$	Moment covariance matrix
$M^{(m)}$	m-th order spatial moment of M
M_0	Seismic moment
M_{kl}	Moment tensor
m_i	i-th mass
q_c	Spatial moment centroid
$\mathbf{R}$	Center of gravity
r_i	i-th distance
$T^{(m,n)}$	m-th order spatial moment n-th order temporal moment of T
T_i	Traction along i direction
u_i	Displacement along i direction
$\mathbf{v}$	Mean rupture velocity
v_i	i-th eigenvector of a matrix
v_j	Fault normal
w	Second order moment where spatial and temporal degree is 1
α	Velocity of P-wave
β	Velocity of S-wave
γ_i	Direction cosine along i direction
$\Delta\tau$	Square root of the second temporal moment
Δt	Mean source duration

ε_{ij}	Strain
η	Spatial variable
η_T	Spatial moment centroid of T
λ	Lamé coefficient
μ	Shear modulus
ξ	Source location
ρ	Mass per unit area
Σ	Fault area
σ	Standard deviation
σ_{ij}	Stress
τ_c	Temporal moment centroid
τ	Source time

LIST OF ACRONYMS/ABBREVIATIONS

1D	One Dimensional
2D	Two Dimensional
3D	Three Dimensional

1. INTRODUCTION

Seismic sources in general are finite in space and time. Backus (1976) stated that if a seismic event does not involve external bodies or forces, its source can be defined as a symmetric tensor field called the stress glut. One representation of stress glut is the moment tensor density which is a tensor defined in space and time and yields the equivalent forces which represent a seismic source.

The simplest expression of seismic sources can be obtained by assuming them as point sources which is only valid at much longer wavelengths with respect to the source size. In this case moment tensor becomes a symmetric matrix which is localized to a point in space and its time dependence is usually represented by a simple functional shape such as a triangle or a boxcar function [2, 3].

In order to go beyond the point source approximation, we need to study higher frequencies of the source. One way to study the detailed properties of earthquakes is to perform finite fault kinematic models. In the finite fault method, earthquakes are modeled by dividing a large fault into a collection of elementary subfaults. This type of models provide information about spatial and temporal variation on the fault [4]. Synthetic seismograms are computed by summing the contributions of individual subfaults [5]. One can obtain slip distribution, rupture velocity and rise time (duration of slip at a certain point on fault) by modeling the near source seismic and geodetic data and teleseismic waveforms. One drawback of finite fault kinematic models is that a fault geometry has to be defined a priori to the modeling. In addition, in order to obtain reliable slip distributions seismic and geodetic data from nearby stations need to be available and multiple Green's functions calculations needs to be performed. These increase the time to obtain a finite fault model.

Another method which can be used to obtain first order finite fault parameters is higher order moments method, which relies on the Taylor expansion of representation theorem and keeping the terms up to degree 2 [6, 7]. Using this method one can obtain information on the

earthquake source such as differentiation of the fault plane from the auxiliary plane, size of the rupture, rupture velocity and average duration of the source.

The advantage of this method is that it is relatively simple with less number of unknowns and requires only the spatial and temporal derivatives of one Green's function from the centroid of the source to the receiver.

Stress glut moments and their relations to characteristics of faults have been investigated by Backus [6]. Bukchin [7] studied the determination of stress glut moments from teleseismic surface waves and Clévédé et al. [8] determined the fault parameters of 1999 İzmit earthquake using stress glut moment estimates.

The main objective of this study is exploring how well we can represent a finite fault model in terms of its higher order moments. Specifically, we look for best receiver distances, receiver azimuths and frequency ranges to approximate the finite fault solution by comparing the waveforms of a finite source with point source and higher order moment approximations. The study represented in this thesis forms the base of an inverse process to rapidly determine the finite fault parameters after an earthquake.

In chapter 2, we introduce the concept of higher order moments using basic scalar distributions and functions. Afterwards, we expand the definition to vector and tensor distributions. This allows us to give the relationship between the higher order moments and the fault parameters.

Chapter 3 builds the relationship between the displacement at an observation point and a seismic source represented by its higher order moments. First, we write the equation of motion. We introduce the Green's function solution. Subsequently, we define the representation theorem of faults. We conclude this chapter by writing displacement formula in terms of higher order moments of the moment tensor.

Chapter 4 consists of applications of the method. The first step is to develop a program

to calculate the higher order moments of arbitrarily distributed moment tensor densities. In this section we numerically test this code by applying it to well known distributions and comparing the distribution parameters such as variance with the parameters we obtained from the moments. First, we look at a basic scalar function. Then we test the method on line and planar seismic sources. In the following section, we apply the method to compare the seismograms generated by finite fault sources and their higher order moments. We use the infinite homogeneous isotropic medium. We test the method with bilateral and unilateral line sources and a planar source.

Afterwards, we briefly discuss the application in a layered half space. We show some preliminary results and we touch upon the problems we encountered while taking the Green's function derivatives.

In the last chapter, we discuss the results and their implications.

2. HIGHER ORDER MOMENTS

In order to understand the concept of higher order moments we consider simple cases of distributions.

We start by considering discrete and continuous scalar distributions in 1D and 2D and introduce the zero, first and second order moments. We then extend the concept to distribution of vectors and finally tensors.

2.1. Zero Order Moment

Let points represent masses distributed throughout space (for 1D see Figure 2.1, for 2D see Figure 2.2). Then we can think zero order moment, denoted by $M^{(0)}$, as the total mass of the points distributed in space.

$$M^{(0)} = \sum_{i=1}^{n} m_i \tag{2.1}$$

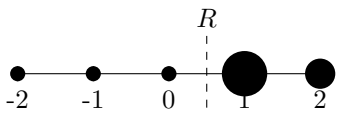

Figure 2.1. 1D mass distribution. R shows the center of gravity.

For the example shown in Figure 2.1, zero order moment will be

$$M^{(0)} = \sum_{i=1}^{n} m_i = 1+1+1+3+2 = 8 \tag{2.2}$$

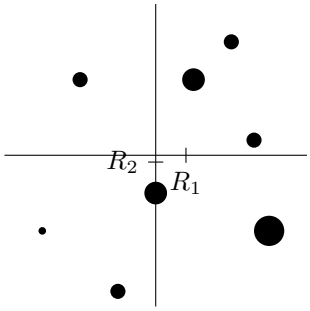

Figure 2.2. 2D mass distribution. R_1 is the center of gravity along *1* (or x) axis and R_2 is the center of gravity along *2* (or y) axis.

For the 2D example in Figure 2.2, zero order moment will be

$$M^{(0)} = \sum_{i=1}^{n} m_i = 1+1+1.5+2+1.5+0.5+1+1 = 9.5 \tag{2.3}$$

In 1D, If the masses are continuously distributed throughout the interval D (or a union of intervals) then the total mass can be found by integrating the mass density function $\rho(x)$ in the domain D, where $\rho(x)$ is the mass per unit length.

$$\rho^{(0)} = \int_D \rho(x)dx \tag{2.4}$$

In 2D, domain is an area (or a union of areas) and $\rho(x,y)$ is the mass per unit area which depends on both x and y.

$$\rho^{(0)} = \iint_D \rho(x,y)dxdy \tag{2.5}$$

2.2. First Order Moment

The concept describes the distance between the selected point and the centroid (center point which will be discussed later) multiplied by the zero order moment.

We can calculate the first moment, denoted by $M^{(1)}$, around the origin for 1D using the following equation.

$$M^{(1)}(0) = \sum_{i=1}^{n} m_i r_i \tag{2.6}$$

where r_i is the distance between the origin and i^{th} the point.

For example, we can calculate first order moment for Figure 2.1 around the origin.

$$M^{(1)}(0) = \sum_{i=1}^{n} m_i r_i = (-2*1) + (-1*1) + (0*1) + (1*3) + (2*2) = 4 \tag{2.7}$$

For an arbitrary point P this equation becomes:

$$M^{(1)}(P) = \sum_{i=1}^{n} m_i (r_i - P) = \sum_{i=1}^{n} m_i r_i - \left(\sum_{i=1}^{n} m_i \right) P = M^{(1)}(0) - M^{(0)} P \tag{2.8}$$

First order moment of a continuous 1D distribution for point P can be calculated using the following equation.

$$\rho^{(1)}(P) = \int_D \rho(x)(x-P)dx \tag{2.9}$$

where $(x-P)$ is the distance between a point and P.

In 2D, we have two axes. Thus, we need to calculate two moments one for each axes. If we write the distance between a point and the origin as vectors, then we can write first order moment of a discrete 2D distribution for a point P as follows:

$$\mathbf{M}^{(1)}(\mathbf{P}) = \sum_{i=1}^{n} m_i(\mathbf{r_i} - \mathbf{P}) = \mathbf{M}^{(1)}(0) - M^{(0)}\mathbf{P} \tag{2.10}$$

For example, we can calculate first order moment for Figure 2.2 around the origin. For this case each component should be calculated separately.

$$\begin{aligned}
\mathbf{M}^{(1)}(\mathbf{0}) &= \sum_{i=1}^{n} m_i \mathbf{r_i} \\
&= (-1,1)*1 + (1,1.5)*1 + (0,-0.05)*1.5 \\
&+ (1.5,-1)*0.2 + (0.5,1)*1.5 + (-1.5,-1)*0.5 \\
&+ (-0.5,-1.8)*1 + (1.3,0.2)*1 \\
&= (3.8,-0.85)
\end{aligned} \tag{2.11}$$

It can be seen that first component is $M_1^{(1)}(0) = 3.8$ and the second component is $M_2^{(2)}(0) = -0.85$.

For continuous 2D distribution, we need to denote which component we are using to calculate the moment. We can write the first order moment of a continuous 2D function for each component using following equations

$$\begin{aligned} \rho_x^{(1)}(P_x,P_y) &= \iint_D \rho(x,y)(x-P_x)dxdy \\ \rho_y^{(1)}(P_x,P_y) &= \iint_D \rho(x,y)(y-P_y)dxdy \end{aligned} \tag{2.12}$$

where superscript denotes the order of the moment and subscripts denote which component is used.

There is a point which the first order moment is zero. We can call this point center of gravity for mass distributions. Let's say center of gravity is $\mathbf{R}$ then first order moment around this point will be zero. In more than one dimension and for discrete case we can write the equation as

$$\mathbf{M}^{(1)}(\mathbf{R}) = \sum_{i=1}^{n} m_i(\mathbf{r_i} - \mathbf{R}) = \mathbf{0} \tag{2.13}$$

If we solve for $\mathbf{R}$, we obtain the the equation below.

$$\mathbf{R} = \frac{\sum m_i \mathbf{r_i}}{\sum m_i} = \frac{\mathbf{M}^{(1)}(0)}{M^{(0)}} \tag{2.14}$$

which says that first order moment at origin divided by zero order moment gives the

point where the first order moment is zero or the center of gravity for mass distributions. We can find the center of gravity for Figure 2.1 by using values we got from equation 2.2 and equation 2.7.

$$R = \frac{M^{(1)}(0)}{M^{(0)}} = \frac{4}{8} = 0.5 \tag{2.15}$$

For Figure 2.2, we can use the values from equation 2.3 and equation 2.11.

$$\mathbf{R} = \frac{\mathbf{M}^{(1)}(0)}{M^{(0)}} = \frac{(3.8, -0.85)}{9.5} = (0.4, -0.09) \tag{2.16}$$

The components of the center of gravity can be found as $R_1 = 0.4$ and $R_2 = -0.09$.

If we know the first order moment around $\mathbf{P}$, we can also use that value by plugging equation 2.10 into 2.14.

$$\mathbf{R} = \frac{\mathbf{M}^{(1)}(0)}{M^{(0)}} = \frac{\mathbf{M}^{(1)}(\mathbf{P}) + M^{(0)}\mathbf{P}}{M^{(0)}} = \frac{\mathbf{M}^{(1)}(\mathbf{P})}{M^{(0)}} + \mathbf{P} \tag{2.17}$$

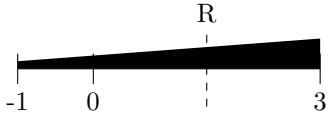

Figure 2.3. Continuous 1D mass distribution. R shows the center of gravity.

For continuous 1D case, let us define density function $\rho(x)$ within domain $x \in [1,3]$.

$\rho(x)$'s graph looks like Figure 2.3. We can find the center of gravity R using the following formula.

$$R = \frac{M^{(1)}(0)}{M^{(0)}} = \frac{\int_{-1}^{3} \rho(x)(x-0)dx}{M^{(0)}} \tag{2.18}$$

where $\rho(x)$ is mass per unit length.

In 2D, center of gravity can be calculated using

$$\mathbf{R} = \frac{(\rho_x^{(1)}(\mathbf{0}), \rho_y^{(1)}(\mathbf{0}))}{\rho^{(0)}} \tag{2.19}$$

where $\rho_x^{(1)}$ and $\rho_y^{(1)}$ are defined in equation 2.12

2.3. Second Order Moment

Zero order moment gives the total mass and we can find center of gravity using first order moment. Second order moment gives the information about mass spread around the center of gravity. Two different distributions can have same total mass and center of gravity (See Figure 2.4). We can differentiate between these two distributions using the second order moment denoted by $f^{(2)}$.

In 1D, second moment of a scalar function can be calculated using the equation 2.20 on the center of gravity.

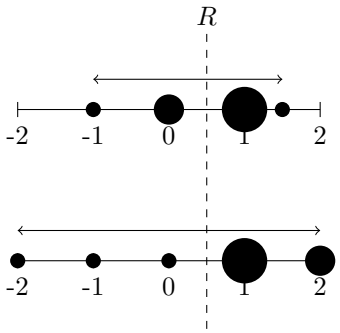

Figure 2.4. Two distributions with same total mass and center of gravity (R) but different spread.

$$f^{(2)}(R) = \int_{-\infty}^{\infty} dx f(R)(x-R)(x-R) \tag{2.20}$$

In 2D, we have 3 different second moments to calculate ($f_{12} = f_{21}$).

$$f_{11}^{(2)}(\mathbf{R}) = \iint_{D} dA f(\mathbf{x}) (x_1 - R_1)^2 \tag{2.21}$$

$$f_{12}^{(2)}(\mathbf{R}) = \iint_{D} dA f(\mathbf{x}) (x_1 - R_1)(x_2 - R_2) \tag{2.22}$$

$$f_{22}^{(2)}(\mathbf{R}) = \iint_{D} dA f(\mathbf{x}) (x_2 - R_2)^2 \tag{2.23}$$

We can write these values as a 2 by 2 matrix.

$$f^{(2)} = \begin{bmatrix} f_{11}^{(2)} & f_{12}^{(2)} \\ f_{21}^{(2)} & f_{22}^{(2)} \end{bmatrix} \tag{2.24}$$

For 3D this matrix will be 3 by 3.

$$f^{(2)} = \begin{bmatrix} f_{11}^{(2)} & f_{12}^{(2)} & f_{13}^{(2)} \\ f_{21}^{(2)} & f_{22}^{(2)} & f_{23}^{(2)} \\ f_{31}^{(2)} & f_{32}^{(2)} & f_{33}^{(2)} \end{bmatrix} \tag{2.25}$$

We can generalize second order moment equation for a point $\mathbf{q}$ and for components k_1 and k_2.

$$f_{x_{k_1}x_{k_2}}^{(2)}(\mathbf{q}) = \int_V dV_x f(\mathbf{x})(x_{k_1} - q_{k_1})(x_{k_2} - q_{k_2}) \tag{2.26}$$

In general, we can write the m-th order moment of a scalar function on n-dimensional space as follows

$$f_{x_{k_1}\ldots x_{k_m}}^{(m)}(\mathbf{q}) = \int_V dV_x f(\mathbf{x})(x_{k_1} - q_{k_1})\ldots(x_{k_m} - q_{k_m}) \tag{2.27}$$

where dV_x is the n-dimensional infinitesimal volume.

2.4. Moment in Time Domain

If a distribution is defined as a finite source in time, we can also calculate the temporal moments of the distribution. In this case, we use time component instead of spatial components. Equation 2.28 shows n degree moment due to time.

$$f^{(0,n)}(\mathbf{q},\tau) = \int_{\Omega} dV_x \int_{0}^{\infty} dt f(\mathbf{x},t)(t-\tau)^n \tag{2.28}$$

For moments in both spatial and temporal domain, we can write the general equation 2.29 [7].

$$f^{(m,n)}_{x_{k_1}\ldots x_{k_n}}(\mathbf{q},\tau) = \int_{\Omega} dV_x \int_{0}^{\infty} dt f(\mathbf{x},t)(t-\tau)^n (x_{k_1}-q_{k_1})\ldots(x_{k_n}-q_{k_n}) \tag{2.29}$$

First moment due to time $f^{(0,1)}$ will give us the time that represents the function best which is analog to center of gravity in spatial domain. Second moment where $m = 1$ and $n = 1$ namely $f^{(1,1)}$ will tell us about the directivity of an earthquake. In 3D case this moment will have three components. We can compare these component values and argue about rupture propagation. Second moment due to time $f^{(0,2)}$ will gives us how function spreads in time domain. The meaning of the moments for an earthquake source will be discussed further in the following sections.

2.5. Moments of Vector-valued Functions and Tensors

Until this point we have worked with discrete and continuous scalar distributions. We can also calculate moments of vector and tensor distributions. Second spatial moment can be written in tensor notation as the equation below [6].

$$\mathbf{T}^{(2,n)}(\mathbf{q},\tau) = \int_{\Omega} dV_x \int_{-\infty}^{\infty} dt(t-\tau)^n \mathbf{T}(\mathbf{x},t) \otimes (\mathbf{x}-\mathbf{q}) \otimes (\mathbf{x}-\mathbf{q}) \tag{2.30}$$

2.5.1. Higher Order Moment of Vector-valued Functions

If $\mathbf{T}$ is a vector valued function defined in 3D space and time as

$$\mathbf{T} : (x_1,x_2,x_3,t) \rightarrow (T_1(x_1,x_2,x_3,t), T_2(x_1,x_2,x_3,t), T_3(x_1,x_2,x_3,t))$$

We can use the component notation to denote the moment equations. Equation 2.31 shows the second spatial moment on 1 component of $\mathbf{T}$ along 1 and 2 component.

$$T^{(2,n)}_{x_1;x_1x_2}(\mathbf{q},\tau) = \int_{\Omega} dV_x \int_{-\infty}^{\infty} dt(t-\tau)^n T_1(\mathbf{x},t)(x_1-q_1)(x_1-q_1) \tag{2.31}$$

If $\mathbf{T}$ is a vector, then zero order moment will be a vector which represents the sum of all vectors. We can find its value using equation 2.32.

$$\mathbf{T}^{(0,0)} = \int_V \mathbf{T}(\mathbf{x}) dV \tag{2.32}$$

In component notation we can write that as:

$$T_{x_i}^{(0,0)} = \int_V T_i(\mathbf{x}) dV \tag{2.33}$$

The first spatial moment of a vector-valued function can be calculated using equation 2.34 which will be a second-rank tensor.

$$\mathbf{T}^{(1,0)}(\mathbf{x_0}) = \int \mathbf{T}(\mathbf{x}) \otimes (\mathbf{x} - \mathbf{x_0}) dV \tag{2.34}$$

Similar to the center of gravity for scalar case, one might be interested in finding an ideal point that best represents the distribution of vectors. If we want to find so-called center of gravity or centroid $\eta_{\mathbf{T}}$, we cannot simply divide first order moment by zero order moment like we did in the scalar case. Because $\mathbf{T}^{(1,0)}$ is a second rank tensor, and $\mathbf{T}^{(0,0)}$ is a one-rank tensor. In general, division of a tensor by vector is not defined.

One way to remedy this situation, is to consider the projection of each individual vector onto the direction of $\mathbf{T}^{(0,0)}$. If we only consider this particular direction, each vector point can be represented by a scalar amplitude given by its projection and a well-defined centroid can be found.

In Figure 2.5, an example is shown for a distribution of vectors where each vector is shown by a solid arrow and their projection onto $\mathbf{T}^{(0,0)}$ as dashed arrows. The mathematical description of finding the centroid $\eta_{\mathbf{T}}$ is given by [6]:

$$\eta_{\mathbf{T}} = \frac{\mathbf{T}^{(1,0)}(\mathbf{0})(\mathbf{T}^{(0,0)})}{\left\|\mathbf{T}^{(0,0)}\right\|^2} = \frac{\int \left(\mathbf{T}((x)) \cdot \mathbf{T}^{(0,0)}\right)(\mathbf{x}-\mathbf{0})}{\left\|\mathbf{T}^{(0,0)}\right\|^2} \tag{2.35}$$

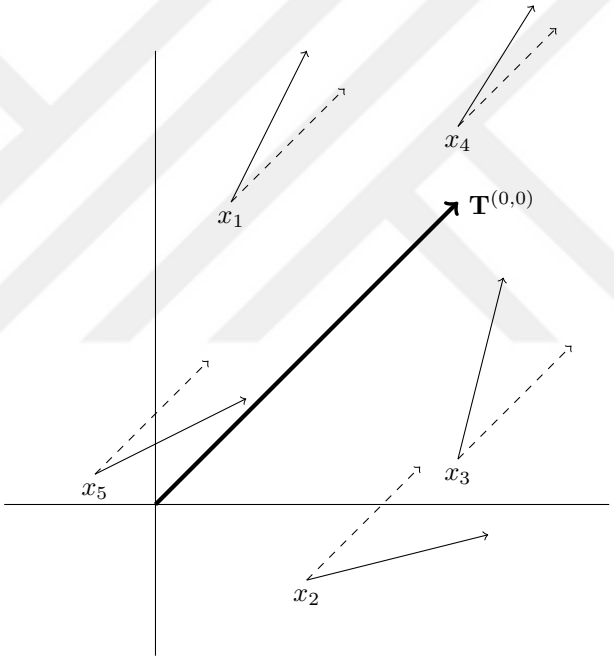

Figure 2.5. Representation of a vector-valued discrete distribution. Solid arrows show individual vector directions. The solid vector at the origin represents the direction and amplitude of zero order moment. The dashed vectors are the projections of each vector to the direction of zero order moment.

We can use the same trick for calculating covariance matrix. In general, $\mathbf{T}^{(2,0)}$ is a third rank tensor so its distribution will depend on which component of the vector we consider. This problem can be avoided by projecting each vector on the direction of $\mathbf{T}^{(0,0)}$ then calculating the second order moment parameters by using the magnitude of the projections which is in effect a scalar distribution. The distribution parameters can be described as a covariance

matrix $\mathbf{K_T}$ as shown in equation 2.36.

$$\mathbf{K_T} = \frac{\mathbf{T}^{(2,0)}(\eta_\mathbf{T})(\mathbf{T}^{(0,0)})}{\left\|\mathbf{T}^{(0,0)}\right\|^2} = \frac{\int(\mathbf{T}(\mathbf{x})\cdot\mathbf{T}^{(0,0)})(\mathbf{x}-\eta_\mathbf{T})\otimes(\mathbf{x}-\eta_\mathbf{T})dV}{\left\|\mathbf{T}^{(0,0)}\right\|^2} \tag{2.36}$$

2.5.2. Higher Order Moments of Second Rank Tensors

If $\mathbf{T}$ is a second rank tensor like the moment tensor density, zero order moment is going to be a second rank tensor, as well.

$$\mathbf{T}^{(0,0)} = \int \mathbf{T}(\mathbf{x})dV_x \tag{2.37}$$

We can find the magnitude of $\mathbf{T}^{(0,0)}$ using equation 2.38.

$$\left\|T^{(0,0)}\right\| = \left\|\int T(x)dV_x\right\| \tag{2.38}$$

First moment of $\mathbf{T}$ with respect to the origin is a third rank tensor given by

$$\mathbf{T}^{(1,0)}(0) = \int \mathbf{T}(\mathbf{x})\otimes(\mathbf{x}-\mathbf{0})dV_x \tag{2.39}$$

As we have seen in the vectoral distribution case, the centroid $\eta_{\mathbf{T}}$ of a tensoral distribution cannot be directly obtained. Therefore, we can find the centroid using the method described for the vector case. We project each tensor onto $\mathbf{T}^{(\mathbf{0},\mathbf{0})}$ and then calculate the first order moment of this scalar distribution. Dot product of two matrices is defined as the sum of multiplication of each components.

$$\eta_{\mathbf{T}} = \frac{\int \left(\mathbf{T}(\mathbf{x}) \cdot \mathbf{T}^{(0,0)}\right)(\mathbf{x}-\mathbf{0})dV_x}{\left\|\mathbf{T}^{(0,0)}\right\|^2} \tag{2.40}$$

In a similar fashion, covariance matrix $\mathbf{K}_{\mathbf{T}}$ for the tensor case can be calculated using equation 2.41.

$$\mathbf{K}_{\mathbf{T}} = \frac{\int (\mathbf{T}(x) \cdot \mathbf{T}^{(0,0)})(\mathbf{x}-\eta_{\mathbf{T}}) \otimes (\mathbf{x}-\eta_{\mathbf{T}})dV}{\left\|\mathbf{T}^{(0,0)}\right\|^2} \tag{2.41}$$

Equivalently we can write the covariance matrix of a tensoral distribution as

$$\mathbf{K}_{\mathbf{T}} = \frac{\mathbf{T}^{(2,0)}(\eta_{\mathbf{T}})(\mathbf{T}^{(0,0)})}{\left\|\mathbf{T}^{(0,0)}\right\|^2} \tag{2.42}$$

2.6. Relations Between Higher Order Moments and Fault Parameters

Let us denote the moment tensor density as $\mathbf{M}(\mathbf{x},t)$. We can find the total seismic moment $\mathbf{M}_0$ by calculating zero order moment.

$$\mathbf{M}_0 = \mathbf{M}^{(0,0)} \tag{2.43}$$

Higher order moments works only for positive distributions. We need to introduce a positivity requirement. We can do that by evaluating each moment tensor density value at $\mathbf{M}^{(0,0)}$ as we did in previous sections. This will produce a scalar distribution as in equation 2.44. If this distribution is a non-zero and non-negative, we say that requirement for positivity is met.

$$f(\mathbf{x},t) = \mathbf{M}(\mathbf{x},t) \cdot \mathbf{M}^{(0,0)} \tag{2.44}$$

Here $f(x,t)$ is a scalar distribution function which scales with projection of moment tensor density at each point to the zero order moment.

Once the representation of the tensoral distribution is confined to a scalar one, one can define the centroid and covariance of the distribution. The centroid location which is the best point source representation point of the distribution can be obtained from equation 2.40 [7]. Note that, the centroid point is not necessarily the hypocenter, but it is the point that is most representative of the distribution.

$$\mathbf{q_c} = \eta_\mathbf{T} = \frac{f^{(1,0)}(\mathbf{0},0)}{f^{(0,0)}} \tag{2.45}$$

We can also find the time centroid τ_c using the equation 2.46.

$$\tau_c = \frac{f^{(0,1)}(\mathbf{0},0)}{f^{(0,0)}} \tag{2.46}$$

The mean source duration Δt can be estimated by $2\Delta\tau$ where $\Delta\tau$ is defined as:

$$(\Delta\tau)^2 = \frac{f^{(0,2)}(\mathbf{q_c},\tau_c)}{f^{(0,0)}} \tag{2.47}$$

Eigenvalues and eigenvectors of the covariance matrix $\mathbf{K_T}$ (equation 2.42) give information about the orientation and size of the source. For example, for a volume source by using the covariance matrix, one can obtain best fitting ellipsoid for a given distribution.

$$\mathbf{K_T} = \frac{f^{(2,0)}(\mathbf{q_c},\tau_c)}{f^{(0,0)}} \tag{2.48}$$

Up to know we have considered second order moments where moment is only in the spatial or temporal domain. One can obtain information about source parameters like directivity using second order moment where $m = 1$ and $n = 1$. In the case of purely unilateral rupture one can also obtain the rupture velocity.

$$\mathbf{w} = \frac{f^{(1,1)}(\mathbf{q_c},\tau_c)}{f^{(0,0)}} \tag{2.49}$$

Mean rupture velocity v is given by the equation 2.50.

$$\mathbf{v} = \frac{\mathbf{w}}{(\Delta\tau)^2} \tag{2.50}$$

3. REPRESENTING DISPLACEMENTS DUE TO AN EARTHQUAKE SOURCE BY HIGHER ORDER MOMENTS

In this chapter, we first write the equation of motion and present the Green's function solution. Afterwards, representation theorem is derived from the equation of motion. Finally, we obtain the representation theorem in terms of higher order moments using the Taylor expansion around a source point.

3.1. Equation of Motion

We can write the equation of motion using the Newton's second law. Mass (ρ) times acceleration ($\ddot{u}_i$) (second derivative of displacement due to time) equals to total force. There are two forces acting on the medium interior *body forces* f_i and *stresses* σ_{ij} on the boundaries. Therefore, we can write equation 3.1 using Einstein's summation convention.

$$\rho(\mathbf{x})\ddot{u}_i = f_i(\mathbf{x},t) + \sigma_{ij,j} \tag{3.1}$$

The deformation or *strain* (ε) in the medium depends on derivatives of displacements.

$$\varepsilon_{kl} = \frac{1}{2}\left(u_{k,l} + u_{l,k}\right) \tag{3.2}$$

From Hooke's law, we can write the relationship between strain and stress where C_{ijkl} is a fourth rank tensor which represents elastic parameters of the medium.

$$\sigma_{ij} = C_{ijkl}\varepsilon_{kl} = C_{ijkl}u_{k,l} \tag{3.3}$$

If we plug 3.3 into 3.1, we can write the wave equation as:

$$\rho\ddot{u}_i = f_i + C_{ijkl}u_{k,lj} \tag{3.4}$$

3.1.1. Green's function solution

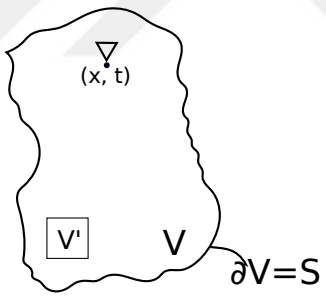

Figure 3.1. Representation of domain (V), boundary (∂V), measurement point ((x,t)) and source region (V').

Assume that for unit impulse ($\delta(\mathbf{x}-\mathbf{x_0})(t-t_0)$), response function is know which is $G(\mathbf{x},t;\mathbf{x_0},t_o)$.

Solution to the wave equation is stable and unique if we have

(i) Initial condition for all $x \in V$ $u(\mathbf{x},t_0)$ and $\dot{u}(\mathbf{x},t_0)$

(ii) A boundary condition

- $u(\mathbf{x},t)$ is given for all $x \in \partial V$ *or*

- Traction vector $T_i(u)$ is given ($T_i(u) = \sigma_{ij} n_j = C_{ijkl} u_{k,l} n_j$)

If we have these conditions we can write the general solution of wave equation as:

$$u_n(\mathbf{x},t) = \int_{-\infty}^{\infty} \iiint_V f_i G_{ni} dV d\tau + \int_{-\infty}^{\infty} \iint_S u_i T_i(G) dS d\tau + \int_{-\infty}^{\infty} \iint_S T_i(u) G_{ni} dS d\tau \tag{3.5}$$

If the traction $\mathbf{T}(u)$ boundary condition is given, then the second term vanishes. If the displacement boundary condition is given, then third term vanishes. First term will give us displacement due to body force. Second and third term give us boundary's contribution to displacement.

3.2. Representation Theorem for Faults

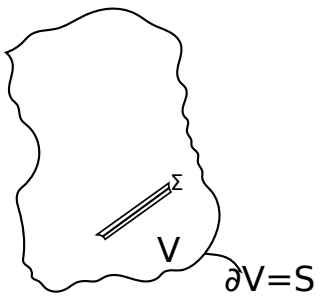

Figure 3.2. Representation theorem for faults. Sigma denotes the fault area. V is the domain volume and dV is the boundary of the domain.

For the case where the body force is zero, we can define a fault as an internal boundary where displacement is discontinuous and tractions are continuous. We will use $[u_i] = u_i^+(\mathbf{x},t) - u_i^-(\mathbf{x},t)$ notation to represent the slip discontinuity at the fault surface. Traction at surface of the earth will be zero. We will denote the fault area by Σ, location in the fault area

by ξ and source times as τ [3].

$$u_n(\mathbf{x},t) = \int_{-\infty}^{\infty} \iint_{\Sigma} [u_i](\xi,\tau) C_{ijkl} \nu_j \frac{\partial G_{nk}}{\partial \Sigma_l}(\mathbf{x},t;\xi,\tau) d\Sigma d\tau \tag{3.6}$$

Green's function has shifting property with respect to time meaning that as long as the difference between observation time and source time is $t-\tau$ we can change the time variables.

$$G_{ni}(x,t;\xi,\tau) = G_{ni}(x,t-\tau;\xi,0) \tag{3.7}$$

If we write Green's function as the right side of 3.7, we can represent time integral as a convolution.

$$f(t) * g(t) = \int_{-\infty}^{\infty} f(\tau) g(t-\tau) d\tau \tag{3.8}$$

Then 3.6 becomes:

$$u_n(\mathbf{x},t) = \iint_{\Sigma} [u_i](\xi,\tau) C_{ijkl} \nu_j * G_{nk,l}(\mathbf{x},t;\xi,\tau) d\Sigma_{(\xi)} \tag{3.9}$$

3.2.1. Equivalent body force

In order to find the equivalent body forces, we need to get rid of the Green's function derivative in equation 3.9.

Equation 3.9 yields the displacement at a receiver point by integrating the slip on the fault plane. We can write the integral as a volume integral for whole region instead of only for the fault region by adding a dirac delta term to the equation which is zero outside the Σ region ($\delta(\Sigma)$) [3]. The spatial variable for source ξ will change to η.

$$u_n(\mathbf{x},t) = \iiint_V ([u_i](\xi,\tau)C_{ijkl}\nu_j\delta(\Sigma)) * G_{nk,l}(\mathbf{x},t;\eta,\tau)dV_{(\eta)} \tag{3.10}$$

We can get rid of Green's function's derivative using integration by parts. First term will be zero because evaluation of Green's function with dirac delta at boundaries vanishes ($\delta(\Sigma)$ is zero at ∂V outer surface of V). Therefore, equation can be written as in 3.11.

$$u_n(\mathbf{x},t) = -\iiint_V \frac{\partial}{\partial\eta_l}([u_i](\xi,\tau)C_{ijkl}\nu_j\delta(\Sigma)) * G_{nk}(\mathbf{x},t;\eta,\tau)dV_{(\eta)} \tag{3.11}$$

The term $-\frac{\partial}{\partial\eta_l}([u_i](\xi,\tau)C_{ijkl}\nu_j\delta(\Sigma))$ is the equivalent body force for the fault. And the term $[u_i](\xi,\tau)C_{ijkl}\nu_j$ equals to moment tensor M_{kl}. Then, we can we say that equivalent body force for an earthquake equals to divergence of moment tensor ($M_{kl,l} = \nabla \cdot M_{kl}$).

3.3. Writing Displacement in Terms of Moment Tensor's Moments

The relation between the displacement field at the observation point and the moment tensor at the source point is given by the following expression [3].

$$u_n(x,t) = \int_{-\infty}^{\infty} \int_{\Sigma} M_{kl}(\xi,\tau) G_{nk,l}(x,t;\xi,\tau) d\Sigma d\tau \tag{3.12}$$

The Taylor expansion of the Green's function around the source point $\bar{\xi}$ and time $\bar{\tau}$ can be written as

$$
\begin{aligned}
G_{nk,l}(x,t;\xi,\tau) = {} & G_{nk,l}(x,t;\bar{\xi},\bar{\tau}) \\
& + G_{nk,l1}(x,t;\bar{\xi},\bar{\tau})(\xi_1-\bar{\xi}_1) \\
& + G_{nk,l2}(x,t;\bar{\xi},\bar{\tau})(\xi_2-\bar{\xi}_2) \\
& + G_{nk,l3}(x,t;\bar{\xi},\bar{\tau})(\xi_3-\bar{\xi}_3) \\
& + \dot{G}_{nk,l}(x,t;\bar{\xi},\bar{\tau})(\tau-\bar{\tau}) \\
& + \frac{1}{2!}G_{nk,l11}(x,t;\bar{\xi},\bar{\tau})(\xi_1-\bar{\xi}_1)^2 \\
& + G_{nk,l12}(x,t;\bar{\xi},\bar{\tau})(\xi_1-\bar{\xi}_1)(\xi_2-\bar{\xi}_2) \\
& + G_{nk,l13}(x,t;\bar{\xi},\bar{\tau})(\xi_1-\bar{\xi}_1)(\xi_3-\bar{\xi}_3) \\
& + \frac{1}{2!}G_{nk,l22}(x,t;\bar{\xi},\bar{\tau})(\xi_2-\bar{\xi}_2)^2 \\
& + G_{nk,l23}(x,t;\bar{\xi},\bar{\tau})(\xi_2-\bar{\xi}_2)(\xi_3-\bar{\xi}_3) \\
& + \frac{1}{2!}G_{nk,l33}(x,t;\bar{\xi},\bar{\tau})(\xi_3-\bar{\xi}_3)^2 \\
& + \dot{G}_{nk,l1}(x,t;\bar{\xi},\bar{\tau})(\xi_1-\bar{\xi}_1)(\tau-\bar{\tau}) \\
& + \dot{G}_{nk,l2}(x,t;\bar{\xi},\bar{\tau})(\xi_2-\bar{\xi}_2)(\tau-\bar{\tau}) \\
& + \dot{G}_{nk,l3}(x,t;\bar{\xi},\bar{\tau})(\xi_3-\bar{\xi}_3)(\tau-\bar{\tau}) \\
& + \frac{1}{2!}\ddot{G}_{nk,l}(\bar{\xi},\bar{\tau})(\tau-\bar{\tau})^2+\cdots
\end{aligned}
\tag{3.13}
$$

Substituting equation 3.13 in equation 3.12 will give us the displacement at a receiver point in terms of the Green's function its derivatives.

$$
\begin{aligned}
u_n = {} & \int_{-\infty}^{\infty}\int_{\Sigma} M_{kl}G_{nk,l}(x,t;\bar{\xi},\bar{\tau})d\Sigma d\tau + \int_{-\infty}^{\infty}\int_{\Sigma} M_{kl}G_{nk,l1}(x,t;\bar{\xi},\bar{\tau})(\xi_1-\bar{\xi}_1)d\Sigma d\tau \\
& + \int_{-\infty}^{\infty}\int_{\Sigma} M_{kl}G_{nk,l2}(x,t;\bar{\xi},\bar{\tau})(\xi_2-\bar{\xi}_2)d\Sigma d\tau+\cdots
\end{aligned}
\tag{3.14}
$$

The Green's function terms can be taken to the outside of the integral, since the argument of the Green's functions are independent of the integration variable. Observe that, integration variables are ξ and τ and the Green's functions are evaluated at $(\bar{\xi},\bar{\tau})$. The terms inside the integral are the moments of the moment tensor which were defined in chapter 2. For example:

$$\int_{-\infty}^{\infty}\int_{\Sigma} M_{kl}(\xi_1-\bar{\xi}_1)d\Sigma d\tau = M_{kl;1}^{(1,0)} \tag{3.15}$$

Therefore, we can write the displacement in terms of Green's functions and moment tensor's higher order moments as

$$\begin{aligned}
u_n \approx\ & G_{nk,l}(x,t;\bar{\xi},\bar{\tau})M_{kl}^{(0,0)} \\
& + G_{nk,l1}(x,t;\bar{\xi},\bar{\tau})M_{kl;1}^{(1,0)} + G_{nk,l2}(x,t;\bar{\xi},\bar{\tau})M_{kl;2}^{(1,0)} + G_{nk,l3}(x,t;\bar{\xi},\bar{\tau})M_{kl;3}^{(1,0)} \\
& + \dot{G}_{nk,l}(x,t;\bar{\xi},\bar{\tau})M_{kl}^{(0,1)} \\
& + \frac{1}{2!}G_{nk,l11}(x,t;\bar{\xi},\bar{\tau})M_{kl;11}^{(2,0)} + G_{nk,l12}(x,t;\bar{\xi},\bar{\tau})M_{kl;12}^{(2,0)} + G_{nk,l13}(x,t;\bar{\xi},\bar{\tau})M_{kl;13}^{(2,0)} \\
& \qquad + \frac{1}{2!}G_{nk,l22}(x,t;\bar{\xi},\bar{\tau})M_{kl;22}^{(2,0)} + G_{nk,l23}(x,t;\bar{\xi},\bar{\tau})M_{kl;23}^{(2,0)} \\
& \qquad\qquad + \frac{1}{2!}G_{nk,l33}(x,t;\bar{\xi},\bar{\tau})M_{kl;33}^{(2,0)} \\
& + \dot{G}_{nk,l1}(x,t;\bar{\xi},\bar{\tau})M_{kl;1}^{(1,1)} + \dot{G}_{nk,l2}(x,t;\bar{\xi},\bar{\tau})M_{kl;2}^{(1,1)} + \dot{G}_{nk,l3}(x,t;\bar{\xi},\bar{\tau})M_{kl;3}^{(1,1)} \\
& + \frac{1}{2!}\ddot{G}_{nk,l}(\bar{\xi},\bar{\tau})M_{kl}^{(0,2)},
\end{aligned} \tag{3.16}$$

where we have only considered the terms up to second order. First term is the zero order moment which is related total moment of the earthquake and it can be thought as the point source term. Next four terms are the first order terms which represent the deviation from the centroid. If the $\bar{\xi},\bar{\tau}$ is the centroid of the fault, these terms are going to be zero. Next six terms correspond to the spatial distribution of the fault. Following three terms are related to the directivity of the earthquake in 3D. Last term calculates the effect of the duration of the earthquake.

Equation 3.16 can be written by using the series notation as

$$u_n = \sum_{m=0}^{2} \sum_{n=0}^{2} \frac{1}{m!n!} M_{kl;i_1 \ldots i_m}^{(m,n)} \frac{\partial^n G_{nk,li_1 \ldots i_m}(x,t;\bar{\xi},\bar{\tau})}{\partial \tau^n}, \tag{3.17}$$

where the summation convention is used for the k, l and i indices.

In general, in order for higher order moments expansion to work the distributions need to be localized. However, time dependence of moment is not localized due to static displacement. As a solution, we can rewrite equation 3.12 to work with moment rate instead of moment itself by defining a $H_{nk,l}$ as:

$$H_{n,kl} = -\int G_{nk,l} d\tau = \int G_{nk,l} dt$$

Using these equivalences we can write displacement in terms of H:

$$u_n = -\int_{\Sigma} \left(\int_{-\infty}^{\infty} M_{kl}(\xi,\tau) \frac{\partial H_{nk,l}}{\partial \tau}(x,\xi,t-\tau) d\tau \right) d\Sigma \tag{3.18}$$

We obtain the equation below by doing integration by parts:

$$u_n = -\int_{\Sigma} \left(M_{kl} H_{nk,l}(x,\xi,t-\tau) \Big|_{-\infty}^{\infty} \right) d\Sigma + \int_{\Sigma} \int_{-\infty}^{\infty} \frac{\partial M_{kl}}{\partial \tau} H_{nk,l}(x,\xi,t-\tau) d\tau d\Sigma \tag{3.19}$$

First term will be zero, because static displacement at infinity is zero. This will leave us with:

$$u_n = \int_{\Sigma} \int_{-\infty}^{\infty} \dot{M}_{kl}(\xi,\tau) H_{nk,l}(x,\xi,t-\tau) d\tau d\Sigma \tag{3.20}$$

We can write the Taylor expansion of H at $(\bar{\xi},\bar{\tau})$ (Moments and derivatives are computed around $(\bar{\xi},\bar{\tau})$).

$$\begin{aligned}
u_n = {} & H_{nk,l}\dot{M}^{(0,0)}_{kl} \\
& + H_{nk,l1}\dot{M}^{(1,0)}_{kl;1} + H_{nk,l2}\dot{M}^{(1,0)}_{kl;2} + H_{nk,l3}\dot{M}^{(1,0)}_{kl;3} - \frac{\partial H_{nk,l}}{\partial t}\dot{M}^{(0,1)}_{kl} \\
& + \frac{1}{2!}H_{nk,l11}\dot{M}^{(2,0)}_{kl;11} + H_{nk,l12}\dot{M}^{(2,0)}_{kl;12} + H_{nk,l13}\dot{M}^{(2,0)}_{kl;13} \\
& + \frac{1}{2!}H_{nk,l22}\dot{M}^{(2,0)}_{kl;22} + H_{nk,l23}\dot{M}^{(2,0)}_{kl;23} \\
& + \frac{1}{2!}H_{nk,l33}\dot{M}^{(2,0)}_{kl;33} \\
& - \frac{\partial H_{nk,l1}}{\partial t}\dot{M}^{(1,1)}_{kl;1} - \frac{\partial H_{nk,l2}}{\partial t}\dot{M}^{(1,1)}_{kl;2} - \frac{\partial H_{nk,l3}}{\partial t}\dot{M}^{(1,1)}_{kl;3} + \frac{1}{2!}\frac{\partial^2 H_{nk,l}}{\partial t^2}\dot{M}^{(0,2)}_{kl},
\end{aligned} \tag{3.21}$$

where $\frac{\partial H}{\partial t} = -\frac{\partial H}{\partial \tau}$

Using the series notation and the summation convention equation 3.21 can be rewritten as:

$$u_n = \sum_{m=0}^{2}\sum_{n=0}^{2} \frac{(-1)^n}{m!n!}\dot{M}^{(m,n)}_{kl;i_1\ldots i_m}\frac{\partial^n H_{nk,li_1\ldots i_m}}{\partial t^n} \tag{3.22}$$

This final equation allows us to use the higher order moments of moment tensor density and the Green's functions derivatives to find the displacement. $\bar{\xi}$ will be the spatial centroid and $\bar{\tau}$ will be the temporal centroid value which we will compute using the equations in the previous chapter.

4. EXPERIMENTS AND RESULTS

In this chapter, we first calculate higher order moments of some distributions. Initially we calculate moments of a scalar distribution defined by a function. Then, we calculate moments of line source and planar source. This part is done to test the software that calculates the moments.

In the second section, comparisons between synthetic seismograms generated by finite fault models and higher order moments (using equation 3.22) are made for an infinite homogeneous isotropic media. We also included point source approximations for a measure. Unilateral and bilateral line source and planar source are used for these tests.

Last section in this chapter includes the comparisons we made using multi-layered half space media. We talk about some preliminary results and problems while obtaining the Green's functions derivatives.

Higher order moment are calculated by a program written in *python*. Moments of scalar distributions is computed using Riemann sum. Moments of tensor distributions is evaluated via considering each component as a separate scalar distribution. Centroids and covariance matrices are computed using the formulation in chapter 2. Calculations are vectorized using *numpy* package [9]. Plots are made using *matplotlib* package [10].

Generation of *SAC* files for infinite homogeneous isotropic medium and summing Green's function derivatives is done by using *obspy* package [11]. Plotting and filtering of seismograms is done using *Seismic Analysis Code* software [12].

4.1. Moment Calculation of Various Distributions

4.1.1. Scalar function

For the purpose of testing the method and the code that has been written, we first tried to find moments of a scalar function that is defined in equation 4.1.

$$f(x) = 1 - x^2 - y^2 \tag{4.1}$$

in the domain $x^2 + y^2 \leq 1$ and $f(x) = 0$ outside the domain. We limit the domain in the positive region. This is because moment calculation assumes a positive distribution. Function's graph can be seen in Figure 4.1.

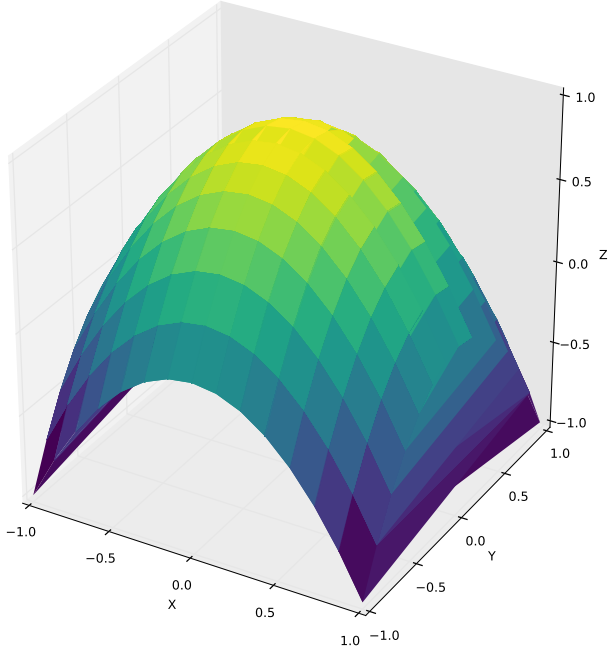

Figure 4.1. 3D plot of the function $f(x) = 1 - x^2 - y^2$ in the domain $x^2 + y^2 \leq 1$.

In order to calculate moments we need to compute the integrals numerically. First we discretize the function (for this example sample rate is $\Delta x = \Delta y = 0.01$) and then we use Riemann sum as defined in equation 4.2 to compute the integrals in the moment functions. For example the zero order moment of the distribution can be calculated by

$$f^{(0,0)} = \int f(x,y)dxdy \approx \sum_{i=1}^{n} f(x_i, y_i)\Delta x \Delta y \tag{4.2}$$

We use the equation 2.4 to calculate the zero order moment. This gives us the result below:

$$f^{(0,0)} = 1.57079320$$

We can check this result computing the corresponding integral analytically

$$\int_{-1}^{1} \int_{-\sqrt{1-y^2}}^{\sqrt{1-y^2}} (1 - x^2 - y^2)dxdy = \frac{\pi}{2} = 1.57079633$$

This gives us error of $E = 1.57079633 - 1.57079320 = 3.12 \times 10^{-6}$ which is acceptable.

Afterwards, if we calculate the first order moment at origin using 2.9 we obtain $(0,0)$. This is expected because function we have selected should have a centroid at the origin.

$$f^{(1,0)}(0,0) = (0.00, 0.00)$$

We also calculated the second moments at the origin. Origin is selected because it is also the spatial centroid.

$$f^{(2,0)}(0,0) = \begin{bmatrix} 2.6180 \times 10^{-1} & -1.8431 \times 10^{-18} \\ -1.8431 \times 10^{-18} & 2.6180 \times 10^{-1} \end{bmatrix}$$

And then we can calculate the eigenvalues and eigenvectors of this matrix. Eigenvalues are:

$$\begin{aligned} e_1 &= 0.26179782 \\ e_2 &= 0.26179782 \end{aligned}$$

And the eigenvectors are:

$$\begin{aligned} v_1 &= (0.7071, 0.7071) \\ v_2 &= (-0.7071, 0.7071) \end{aligned}$$

Note that, eigenvalues are degenerate which means that any direction can be an eigenvector. In Figure 4.2 we plot the function as a contour map and we show eigenvectors of second order moment matrix. These eigenvectors represent the principal axes of the function. Because the function is symmetric around both axes the result we found is consistent with the expectations.

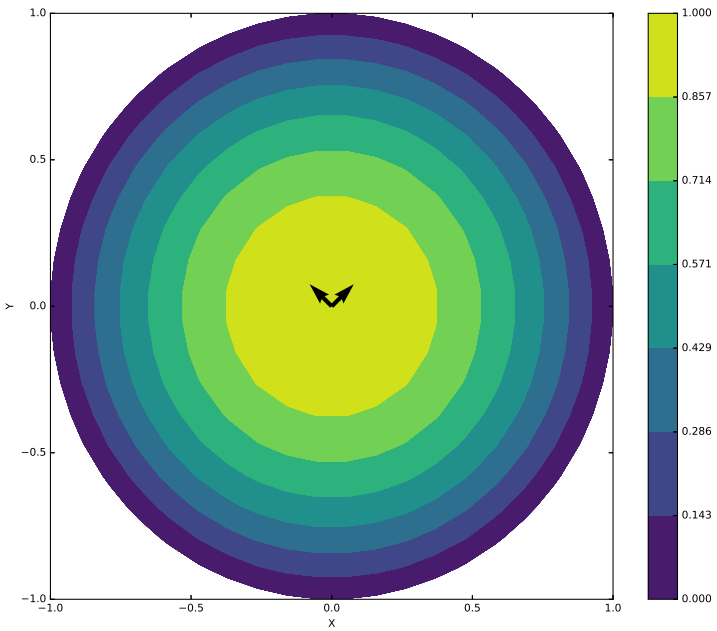

Figure 4.2. Contour map of the bell shaped function. Vectors are the eigenvectors of second order moment matrix. They represent the principal axes of the function.

4.1.2. Line Source

For this test, we define multiple earthquake sources on a line. We define the source type using the formula below.

$$M_{kl} = C_{ijkl} u_i v_j \tag{4.3}$$

where **u** is slip vector, **v** is the fault plane normal and the **C** is the elasticity tensor. For this case, we use the isotropic elasticity tensor which is defined as

$$C_{ijkl} = \lambda(\delta_{ij} + \delta_{kl}) + \mu(\delta_{ik}\delta_{jl} + \delta_{il}\delta_{jk})$$

where λ and μ are the Lamé parameters. For a fault on xy-plane which slip is along x $u = (1,0,0)$, $v = (0,0,1)$ and the $\lambda = \mu = 0.5$ the resulting moment tensor will be:

$$M = \begin{bmatrix} 0 & 0 & 0.5 \\ 0 & 0 & 0 \\ 0.5 & 0 & 0 \end{bmatrix} \tag{4.4}$$

We define the line parametrically starting from the origin and moving along $(1,1)$ direction.

$$L(s) = (0,0) + (1,1)s \tag{4.5}$$

where $s \in [0,5]$. Plot of the line can be seen in Figure 4.3.

Along this line the amplitude of sources are defined by a Gaussian distribution:

$$G(s) = exp\left(\frac{-(s-s_c)^2}{2\sigma^2}\right) \tag{4.6}$$

where $s_c = 2.5$ and $\sigma = 2$. This means that Gaussian is centered at the point $(2.5,2.5)$ which is the center of the line. Plot of the Gaussian source amplitude can be seen in Figure 4.4.

Since this is a seismic source, we also need to define its temporal behavior. For slip rate, we define a trapezoid with the rise time $t_s = 0.2$ and $t_c = 1$. Trapezoid for a point with the arrival time 1 second can be seen in Figure 4.5.

Propagation starts at $(0,0)$ and propagation velocity is $v = 1\ km/s$. We used spatial sampling rate of $dx = dy = 0.05$ and temporal sampling rate of $dt = 0.01$.

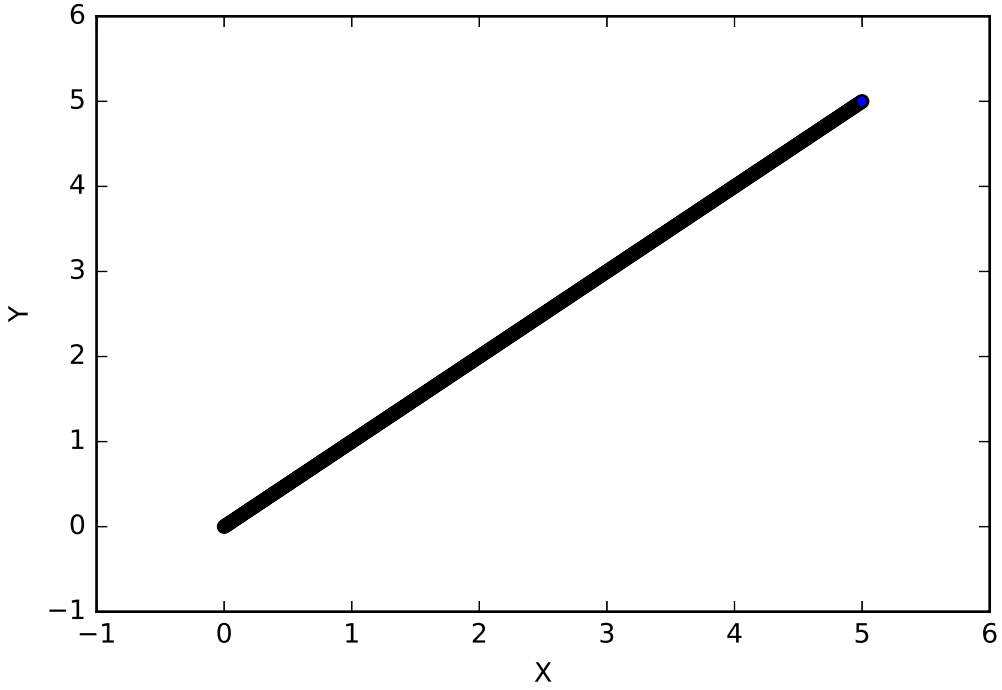

Figure 4.3. Spatial distribution of the sources on a line.

For the defined line source calculated zero order moment is:

$$M^{(0,0)} = \begin{bmatrix} 0 & 0 & 0.11798 \\ 0 & 0 & 0 \\ 0.11798 & 0 & 0 \end{bmatrix}$$

And then we calculated spatial centroid using the equation 2.40.

$$\eta_M = (2.49999, 2.49999)$$

This gives us the expected center point of the line. This is because our amplitude function is

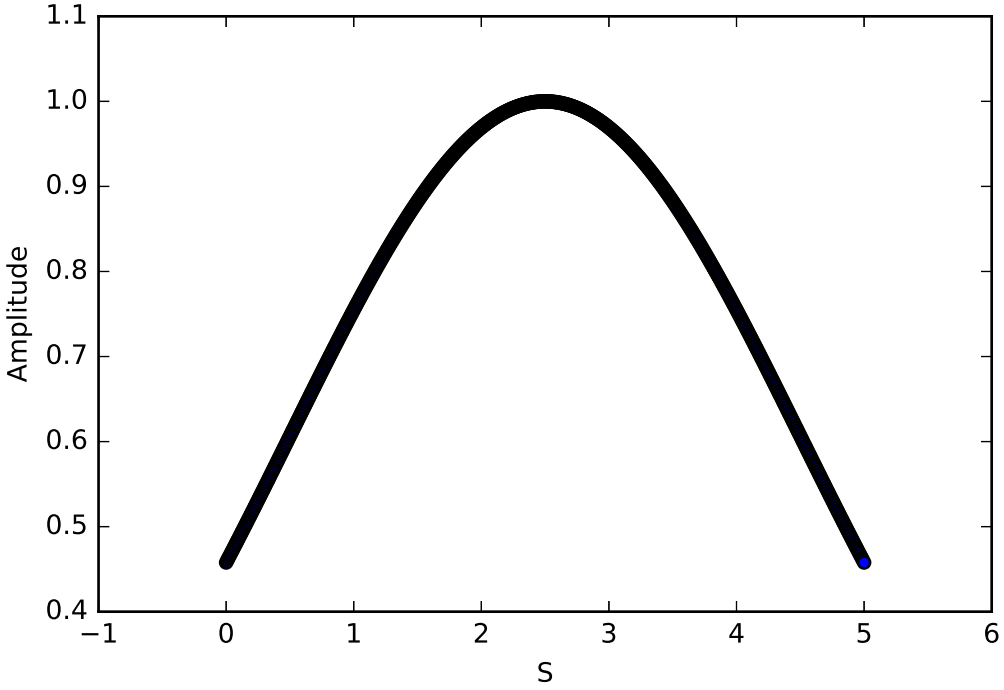

Figure 4.4. Plot of the amplitude function.

Gaussian centered at this point. We also calculated temporal centroid.

$$T_M = 4.2355$$

Total duration of the slip is 8.47 (Arrival time for last point $(5,5)$ is 7.07 and slip time is 1.4). Hence, this result gives the mean time as the best temporal representation point of the source as expected.

We can also find the covariance matrix using equation 2.41.

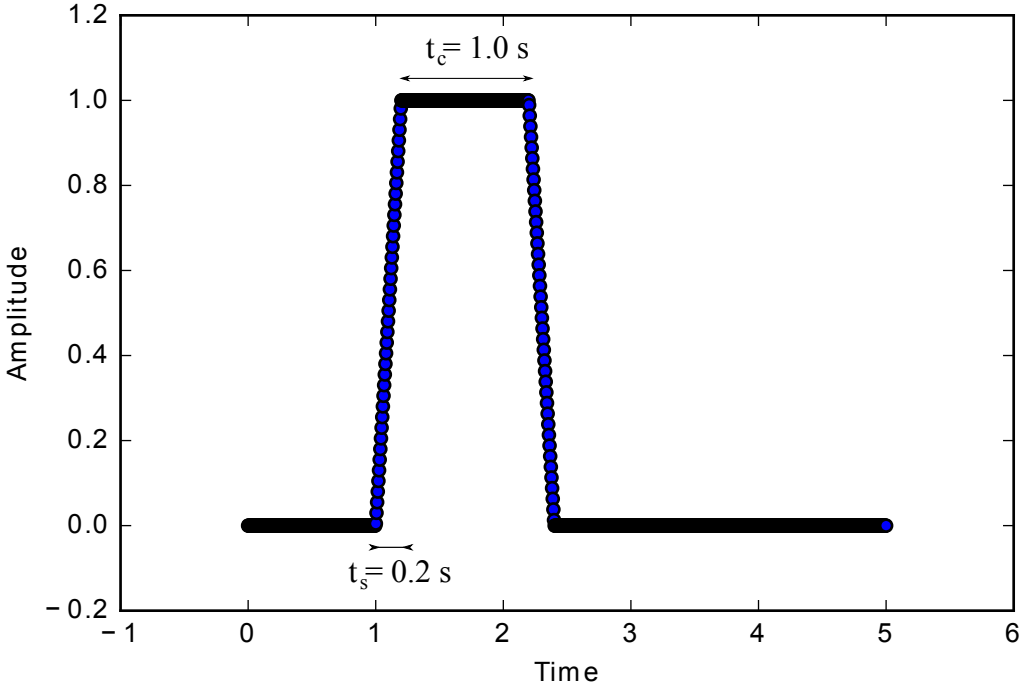

Figure 4.5. Time amplitude function for arrival time 1 second.

$$K_M = \begin{bmatrix} 0.04763 & 0.04763 \\ 0.04763 & 0.04763 \end{bmatrix}$$

If we calculate the eigenvalues we get:

$$e_1 = \quad 0$$

$$e_2 = \quad 0.0953$$

and the eigenvectors are

$$\begin{aligned} v_1 = &\quad (-0.7071, 0.7071) \\ v_2 = &\quad (0.7071, 0.7071) \end{aligned}$$

This says us the distribution along $y = -x$ line is non-existent and correctly states that distribution is only along $y = x$ line.

Source duration can be estimated using second order moment using equation 2.47. It should be noted that this value is the duration after the time centroid. Because the moment is calculated at that time.

$$\begin{aligned} (\Delta\tau)^2 = &\quad 3.55 \\ \Delta\tau = &\quad 1.88 \\ \Delta t = 2\Delta\tau = &\quad 3.77 \end{aligned}$$

We can also calculate the second moment where spatial and temporal moment degree is 1. This gives the information about directivity and rupture velocity in the case of unilateral rupture. Velocity is computed using equation 2.50. Resulting vector is in the same direction of rupture propagation and its amplitude is 0.97 is close to the input value of 1.

$$\mathbf{v} = (0.68, 0.68)$$

4.1.3. Planar source

For this test, we define a plane in 3D which is described parametrically as follows:

$$P(s,t) = (1,1,1) + (1,0,0)s + (0,1,0)t \tag{4.7}$$

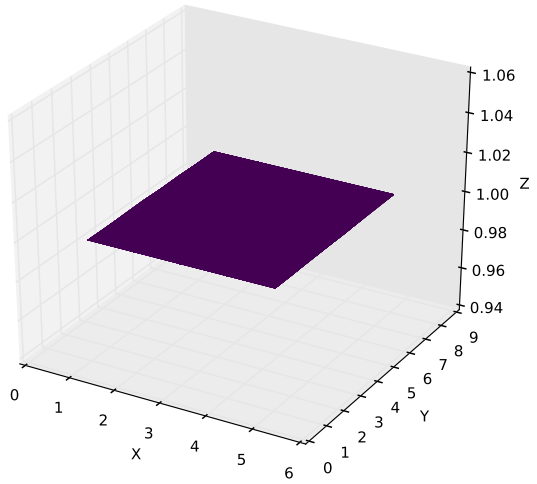

Figure 4.6. Spatial distribution of sources on a plane.

where $s \in [0,5]$ and $t \in [0,8]$. Plot of the plane can be seen in Figure 4.6. We will use the same base moment tensor defined in equation 4.4. Amplitude variation will be handled using a 2D Gaussian defined as:

$$G(s,t) = \exp\left(\frac{-((s,t) - s_c)^2}{2\sigma^2}\right) \tag{4.8}$$

where $s_c = (2.5,4)$ and $\sigma = 2$. Plot of this function can be seen in Figure 4.7

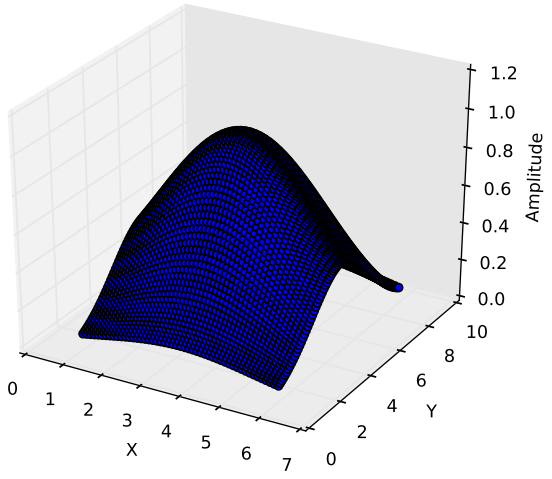

Figure 4.7. Plot of the 2D amplitude function.

For the time domain we use the same slip rate function defined in section 4.1.2. Propagation is only in the y direction and propagation velocity is 1 km/s.

Calculated zero order moment is:

$$M^{(0,0)} = \begin{bmatrix} 0 & 0 & 1.10399 \\ 0 & 0 & 0 \\ 1.10399 & 0 & 0 \end{bmatrix}$$

Computed spatial centroid gives us the result below which is the center of the plane.

$$\eta_M = (3.5, 5, 1)$$

Temporal centroid is

$$T_M = 4.6993$$

Covariance matrix is at the centroid is

$$K_M(\eta_M, T_M) = \begin{bmatrix} 4.2364 & 0 & 0 \\ 0 & 7.6319 & 0 \\ 0 & 0 & 0 \end{bmatrix}$$

Computing the eigenvalues of this second order moment matrix gives us:

$$\begin{aligned} e_1 &= 0 \\ e_2 &= 4.2364 \\ e_3 &= 7.6319 \end{aligned}$$

and the corresponding eigenvectors are:

$$\begin{aligned} v_1 &= (0,0,1) \\ v_2 &= (1,0,0) \\ v_3 &= (0,1,0) \end{aligned}$$

These results correctly describe the distribution as spanned by the x and y direction and the eigenvalue that corresponds to y-direction is greater since plane's length along y-direction is bigger.

The source duration is also computed using second order temporal moment.

$$\begin{aligned}(\Delta\tau)^2 &= 3.25\\ \Delta\tau &= 1.80\\ \Delta t = 2\Delta\tau &= 3.60\end{aligned}$$

Rupture velocity estimated using moment $M^{(1,1)}$ is given below. It is in right direction and it is close the real value $(0,1,0)$.

$$\mathbf{v} = (0, 0.96, 0)$$

4.2. Calculation of Far-field Displacements in Infinite Homogeneous Isotropic Media Using Higher Order Moments

In this section, we calculate far-field displacements due to a moment tensor source distribution and compare with displacement calculated using the higher order moments.

We used whole space Green's functions to test the higher order moment method. Whole space is selected because Green's functions are readily available and their derivative can be taken analytically.

$$G_{ij} = \frac{1}{4\pi\rho}\left[\frac{1}{\alpha^2 r}\gamma_i\gamma_j\delta(t-r/\alpha) - \frac{1}{\beta^2 r}(\gamma_i\gamma_j - \delta_{ij})\delta(t-r/\beta)\right] \tag{4.9}$$

Equation 4.9 shows only the far-field terms of the Green's function for infinite homogeneous isotropic medium [13]. Equation 4.10, 4.11 and 4.12 are the far-field terms of the first, second and third derivatives of the Green's function.

$$G_{ij,k} = \frac{1}{4\pi\rho}\left[\frac{1}{\alpha^3 r}\gamma_i\gamma_j\gamma_k\dot{\delta}(t-r/\alpha) - \frac{1}{\beta^3 r}(\gamma_i\gamma_j\gamma_k - \gamma_k\delta_{ij})\dot{\delta}(t-r/\beta)\right] \tag{4.10}$$

$$G_{ij,kl} = \frac{1}{4\pi\rho}\left[\frac{1}{\alpha^4 r}\gamma_i\gamma_j\gamma_k\gamma_l\ddot{\delta}(t-r/\alpha) - \frac{1}{\beta^4 r}(\gamma_i\gamma_j\gamma_k\gamma_l - \gamma_k\gamma_l\delta_{ij})\ddot{\delta}(t-r/\beta)\right] \tag{4.11}$$

$$G_{ij,klm} = \frac{1}{4\pi\rho}\left[\frac{1}{\alpha^5 r}\gamma_i\gamma_j\gamma_k\gamma_l\gamma_m\dddot{\delta}(t-r/\alpha) - \frac{1}{\beta^4 r}(\gamma_i\gamma_j\gamma_k\gamma_l\gamma_m - \gamma_k\gamma_l\gamma_m\delta_{ij})\dddot{\delta}(t-r/\beta)\right] \tag{4.12}$$

We tested different kind of fault distributions using varying distances and azimuths. For each case, we computed finite fault solution by summing each subfault's contributions. We computed a second set of seismograms with higher order moments using equation 3.22. We used the derivatives of Green's function presented in this section. We also computed another set of seismograms using only zero order moments which is the point source representation. Last computation is done to check the contributions of higher moments to final seismograms. Finally, we compared the seismograms to see how well they agree which each

other at various frequency bands.

4.2.1. Bilateral Line Source

For this case, we have a subfault distribution on a line which consists of 10 subfaults. Line is aligned with north-south direction and it is at the depth of 10 km. Rupture starts at the center and propagates bilaterally. Rupture velocity is 2 km/s. Each subfault is 2x2 km and has an area of 4 km^2. All of subfaults' strike is 0, dip is 0 and rake is 180 degrees and each has 15 cm slip. Sketch of this fault can be seen in Figure 4.8.

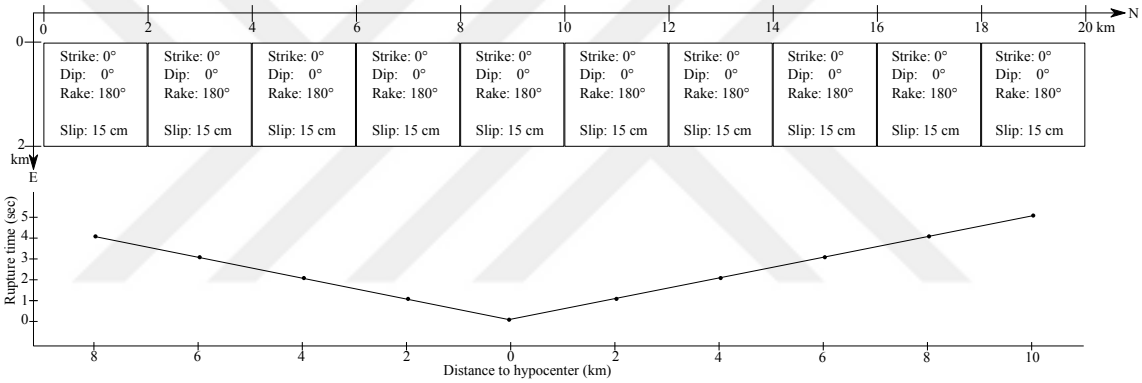

Figure 4.8. Bilateral line source.

Slip rate function is taken from Ji et al, 2003 [14]. Rise time is 0.5 seconds and fall time is 1 second for each subfault (Figure 4.9).

In Figure 4.10 calculated seismograms for receivers at 100 km are represented. Seismograms are arranged according to their azimuths. Black seismograms are from finite fault solutions. Red ones are calculated with only zero order moments and green ones are calculated using higher order moments. Figure 4.11 shows the same comparison for stations at 300 km. Note that, we only consider seismograms along vertical direction. Considering that we are using whole space Green's functions, dip of the fault and distance of the stations we are only observing S waveforms.

It can be seen that neither zero order moment nor higher moment seismograms resem-

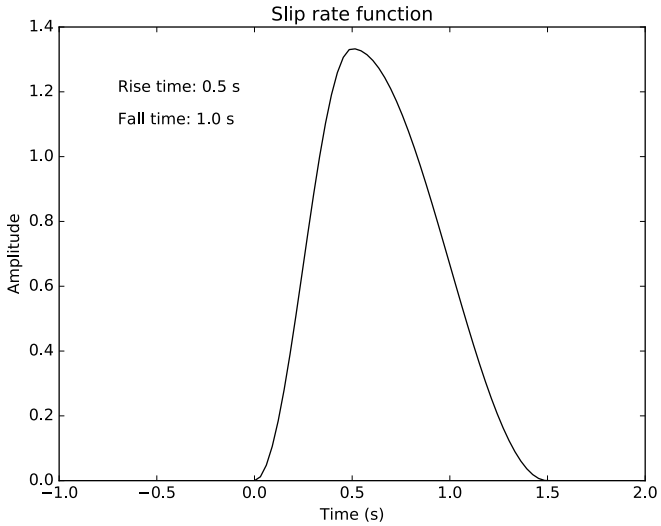

Figure 4.9. Slip rate function.

ble the finite fault one. In order to check for similarities we need to look at specific frequency ranges. Seismograms which are low pass filtered with corner frequency 0.5 Hz can be seen in Figure 4.12. Results are not satisfactory using this filter.

Results for $f_c = 0.25$ Hz low-pass filter can be seen in Figure 4.13. At this range, seismograms start to get similar. However, waveform of zero order moment (red) resembles finite fault solution more than higher order moments. Even though shape of seismograms of higher order moments (green) are not accurate, its wavelength and broadness matches with finite fault more than zero order moments.

Seismograms become comparable when we use low-pass filter with corner frequency 0.1 Hz. Note that this frequency is beyond the corner frequency of the event. This means that at this frequency range it behaves like a point source. Higher order moment solution gives better results than seismograms computed using only zero order moments. Shift in time is present in azimuths 90 degrees and 270 degrees. However, close inspection reveals that the amplitudes of these seismograms are 100 times lower than the other azimuths because they are nodal directions for the displayed S-waves. North-south direction of fault distribu-

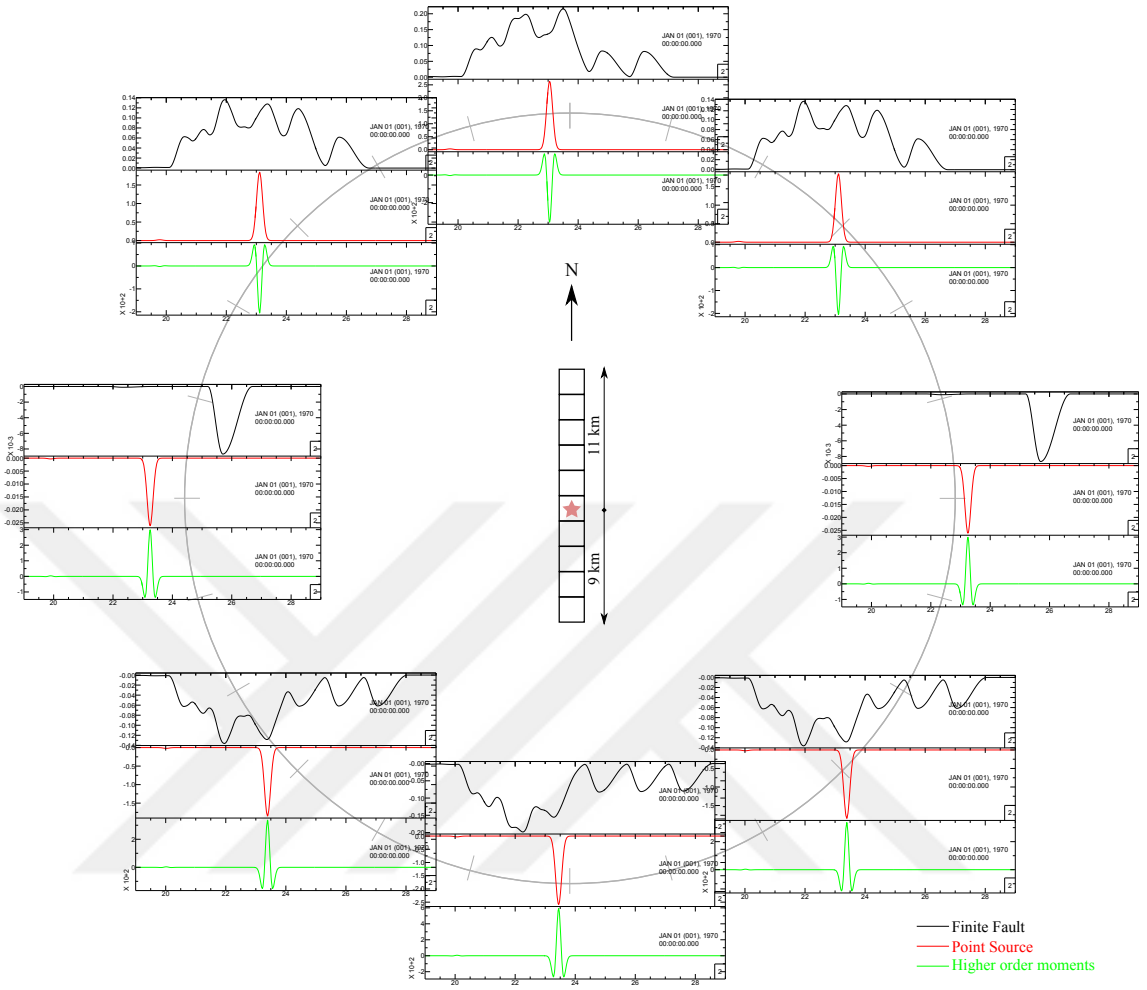

Figure 4.10. Seismograms for receivers at 100 km. Ticks are placed with 15 degrees interval on the circles. At the center fault model is shown. Event starts in the middle and propagates bilaterally.

tion explains the amplitude and lack of variation along west-east direction can explain the inconsistency of moment solutions.

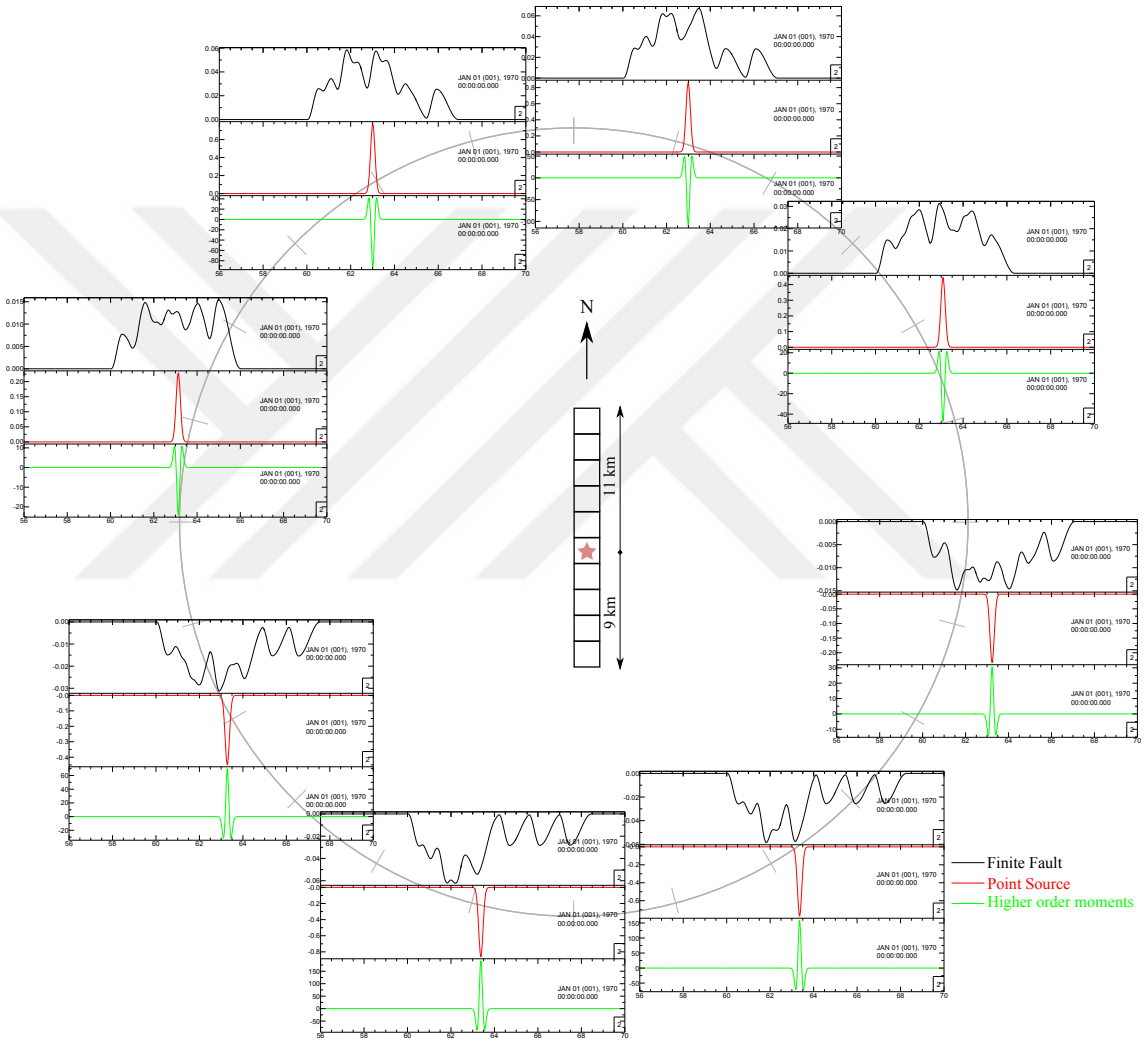

Figure 4.11. Seismograms for receivers at 300 km. Ticks are placed with 15 degrees interval on the circles. At the center fault model is shown. Event starts in the middle and propagates bilaterally.

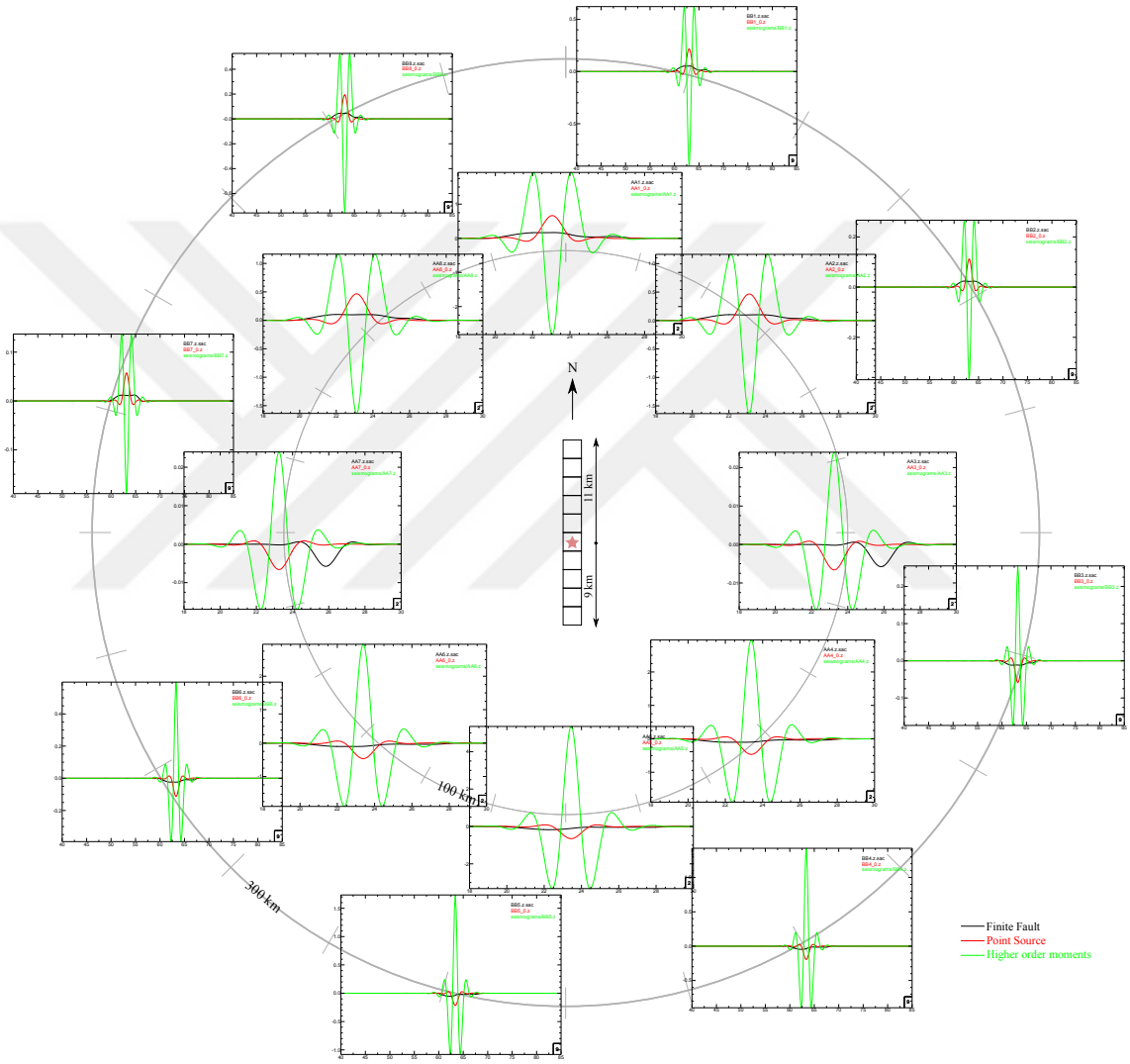

Figure 4.12. Receivers at 100 km and 300 km. Ticks are placed with 15 degrees interval on the circles (Low pass filtered $f_c = 0.5$ Hz). At the center fault model is shown. Event starts in the middle and propagates bilaterally.

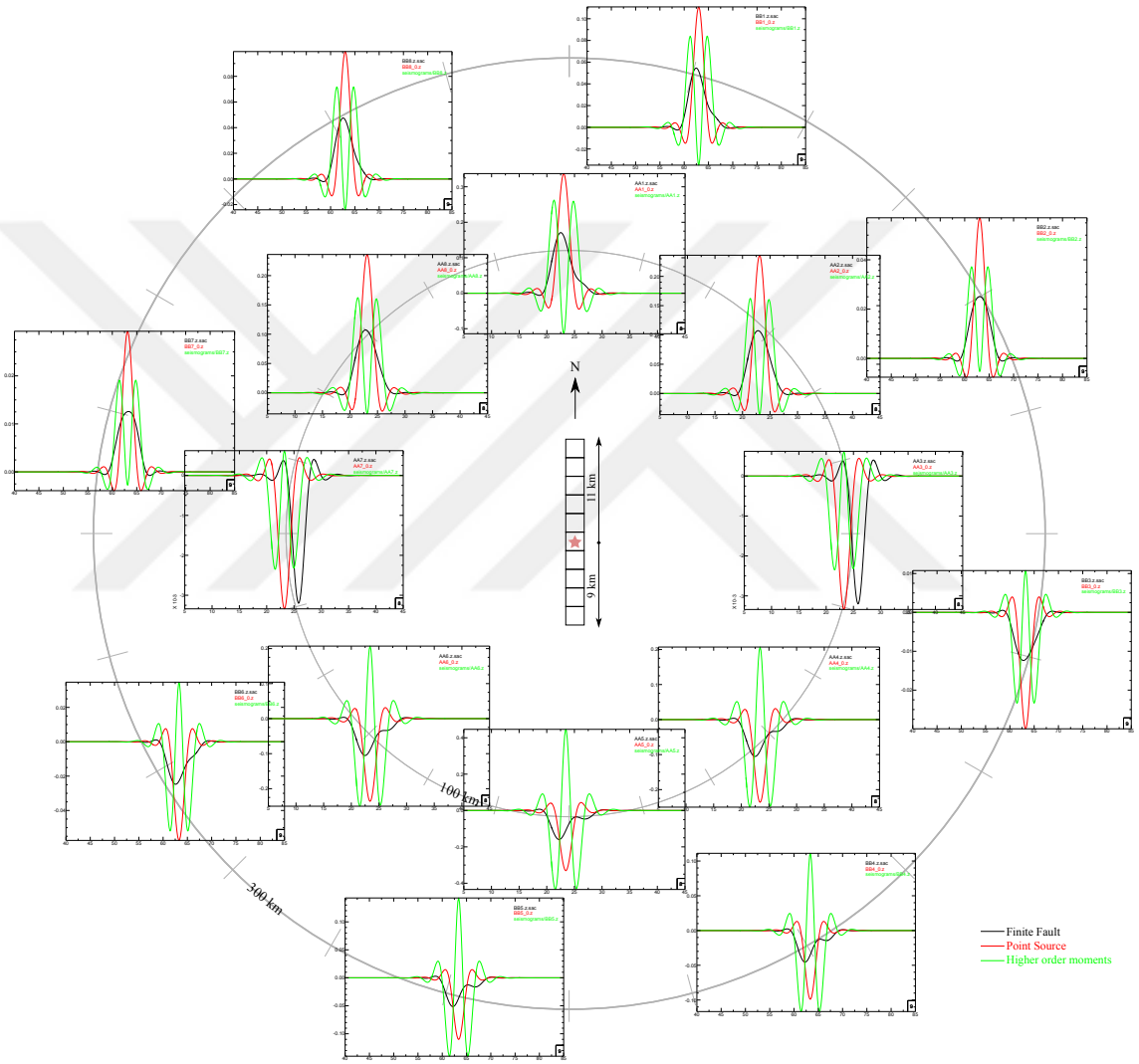

Figure 4.13. Receivers at 100 km and 300 km. Ticks are placed with 15 degrees interval on the circles (Low pass filtered $f_c = 0.25$ Hz). At the center fault model is shown. Event starts in the middle and propagates bilaterally.

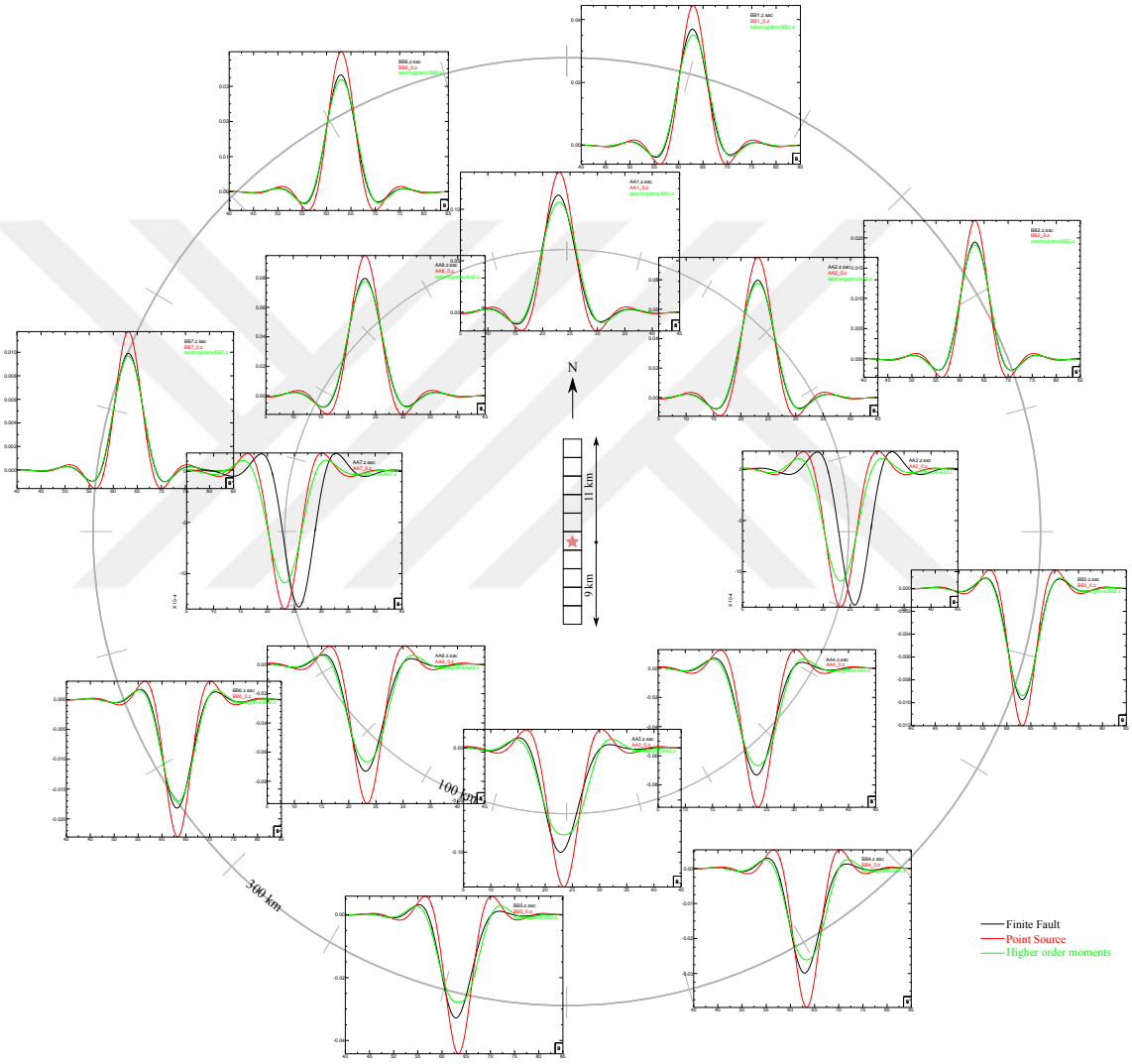

Figure 4.14. Receivers at 100 km and 300 km. Ticks are placed with 15 degrees interval on the circles (Low pass filtered $f_c = 0.1$ Hz). At the center fault model is shown. Event starts in the middle and propagates bilaterally.

4.2.2. Unilateral Line Source

For this case, we have a distribution similar to Section 4.2.1. Except rupture starts at the southmost subfault and propagates unilaterally. Other fault parameters are the same as the previous section. Sketch of this fault can be seen in Figure 4.15.

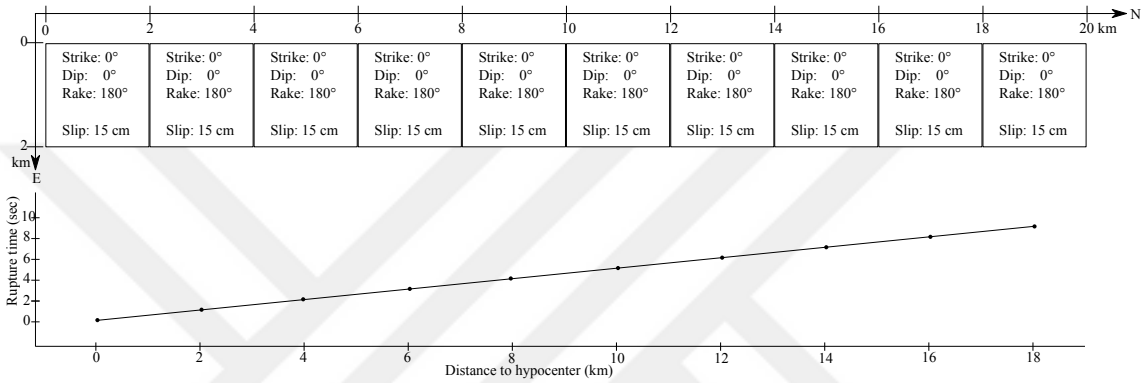

Figure 4.15. Unilateral line source.

Slip rate function is the same with previous section. However, rise and fall times are different. Rise time is 1.0 seconds and fall time is 1.5 seconds for each subfault (see Figure 4.16).

Seismograms for 100 km and 300 km can be seen in Figure 4.17. When we use low-pass filter with corner frequency 0.25 Hz, a direct comparison of waveforms show that the higher order moment waveforms are not similar to the finite fault solution either in terms of waveform shape or amplitude similar to the example shown in the previous section. (See Figure 4.18). However, the pulse broadness are better estimated when higher order moment terms are added.

0.1 Hz low-pass filter gives better results for higher order moments for azimuths 0, 15, 45, 60, 315, 330 degrees which are the receivers in the positive direction of rupture propagation (See Figure 4.19). Effects of directivity can be seen in these directions which result in narrower pulses. Receivers between 90 and 270 degrees have wider pulses. Waveform shapes of the higher order moments for these receivers are not matching with finite fault

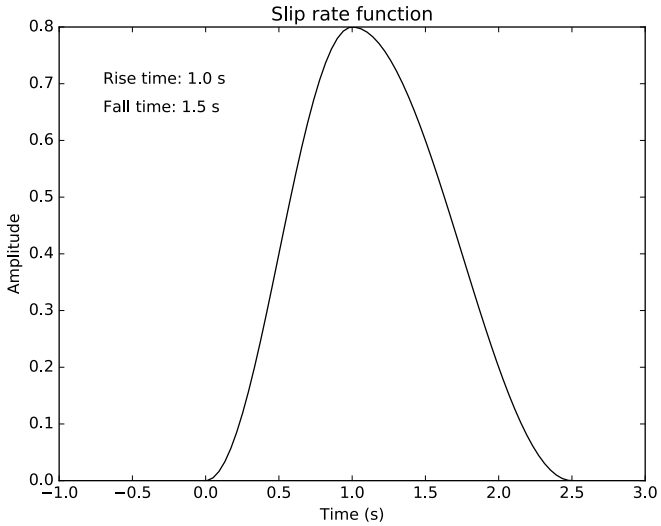

Figure 4.16. Slip rate function for unilateral line source.

ones. However, width of waveforms are matched better with higher order terms.

In Figure 4.20, we can see variation with different filters using a receiver at 500 km with azimuth 190 degrees. It can be seen that higher order moment solutions matches with the length of waveform but not in the waveform shape. Using 0.05 Hz low-pass filter which is beyond the corner frequency of the fault reveals that adding higher order terms improves the result. Amplitude and wavelength of the finite fault result are better matched with the higher order moments solution.

We can also investigate how performance of the higher order moments changes with distance. Figure 4.21, shows two receivers at 100 km and 1000 km with 135 degrees azimuth. Each column represents a receiver, each row has been filtered with different low-pass filters. Waveforms of these two receivers have no significant difference. Only difference is in the amplitudes. This is due to nature of Green's function in infinite homogeneous isotropic medium. Only factor that affects these seismograms to differ are the distances. Hence, seismograms are different in their arrival times and amplitudes which is inversely proportional to distance. This explains the amplitude ratio which is equivalent to distance ratio. Due to

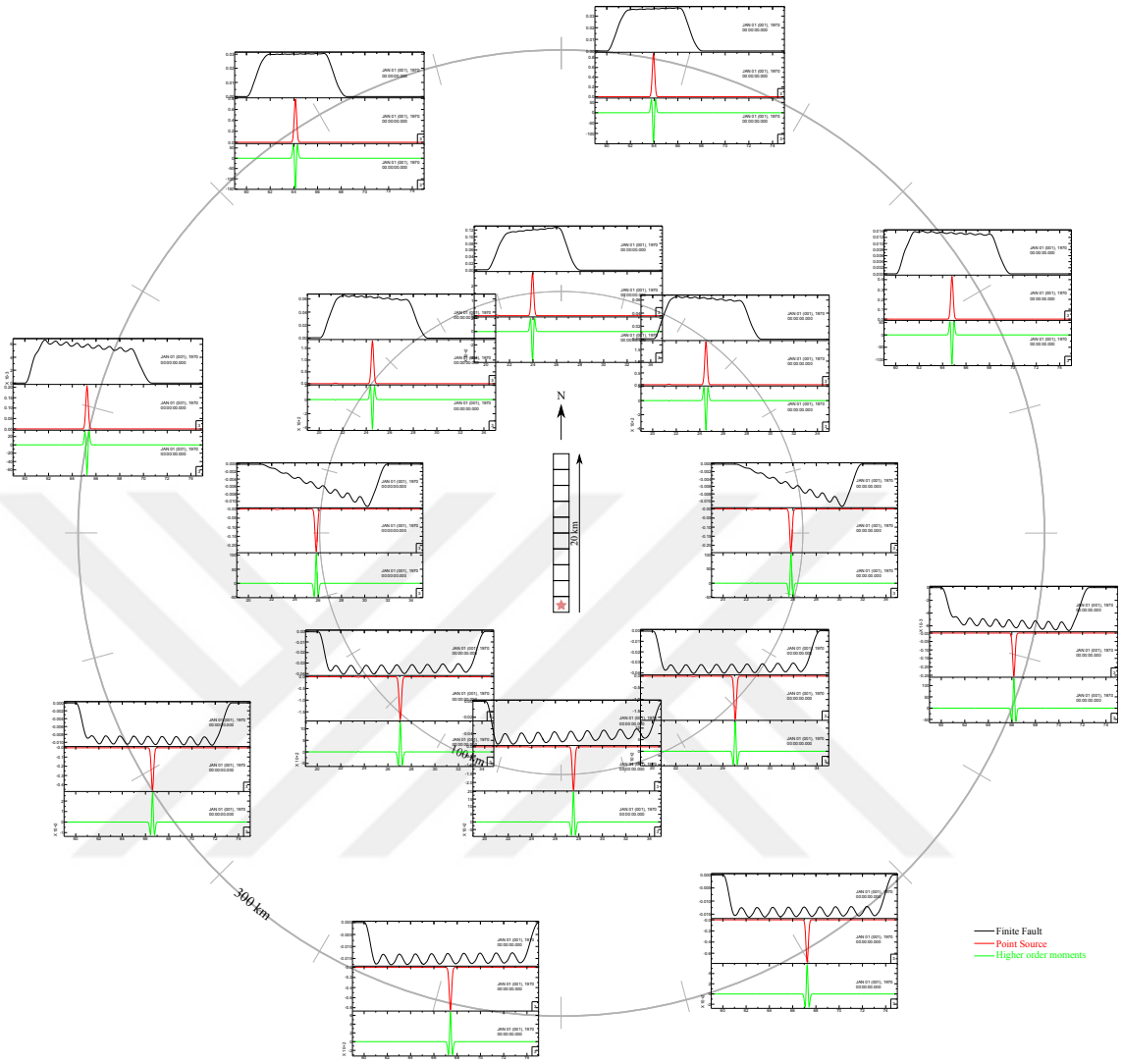

Figure 4.17. Receivers at 100 km and 300 km. Ticks are placed with 15 degrees interval on the circles. At the center fault model is shown. Event starts at the southmost subfault and propagates to the north.

this effect, we cannot differentiate the performance of higher order moments with distance in the whole space.

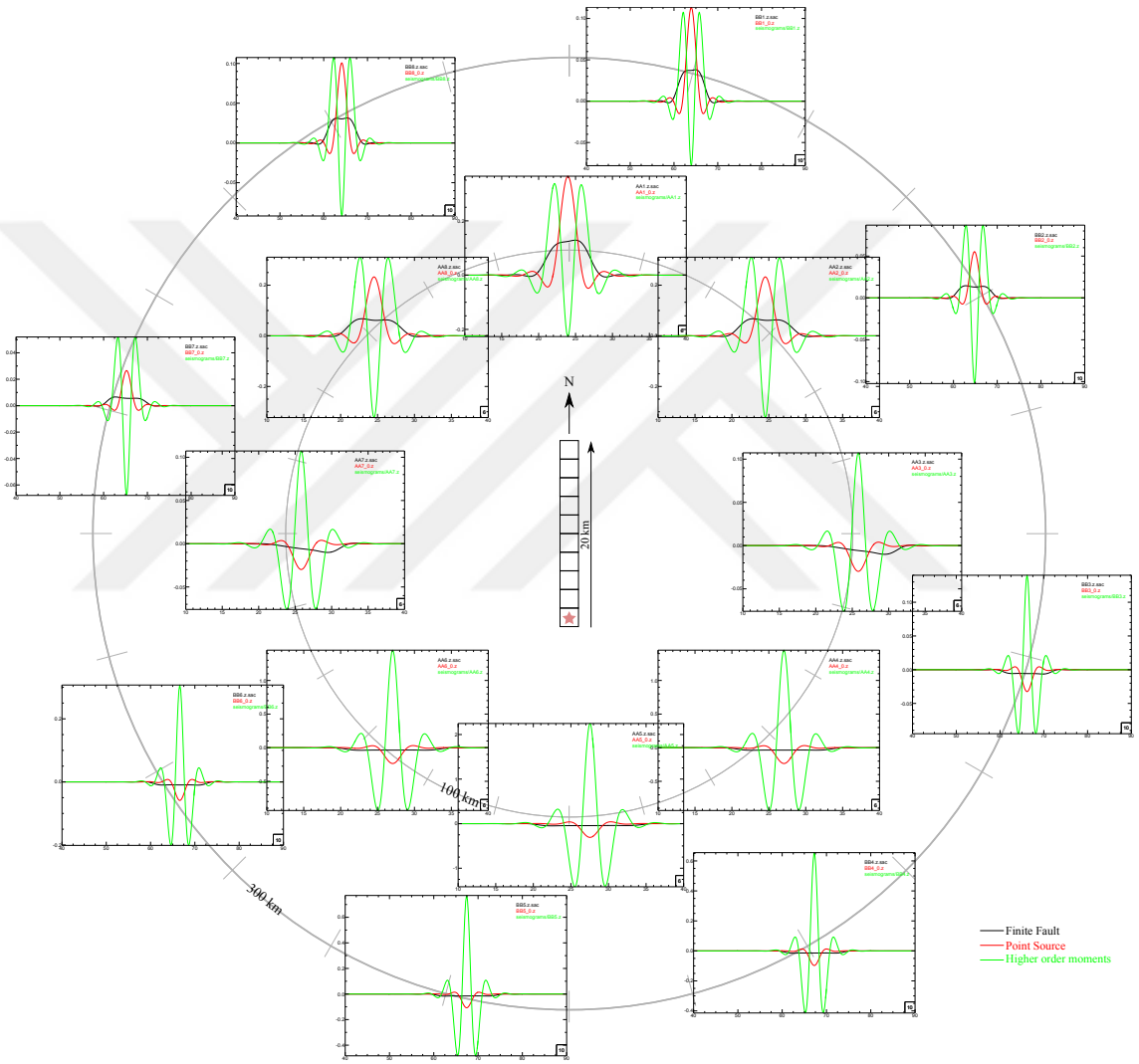

Figure 4.18. Receivers at 100 km and 300 km. Ticks are placed with 15 degrees interval on the circles (Low pass filtered $f_c = 0.25$ Hz). At the center fault model is shown. Event starts at the southmost subfault and propagates to the north.

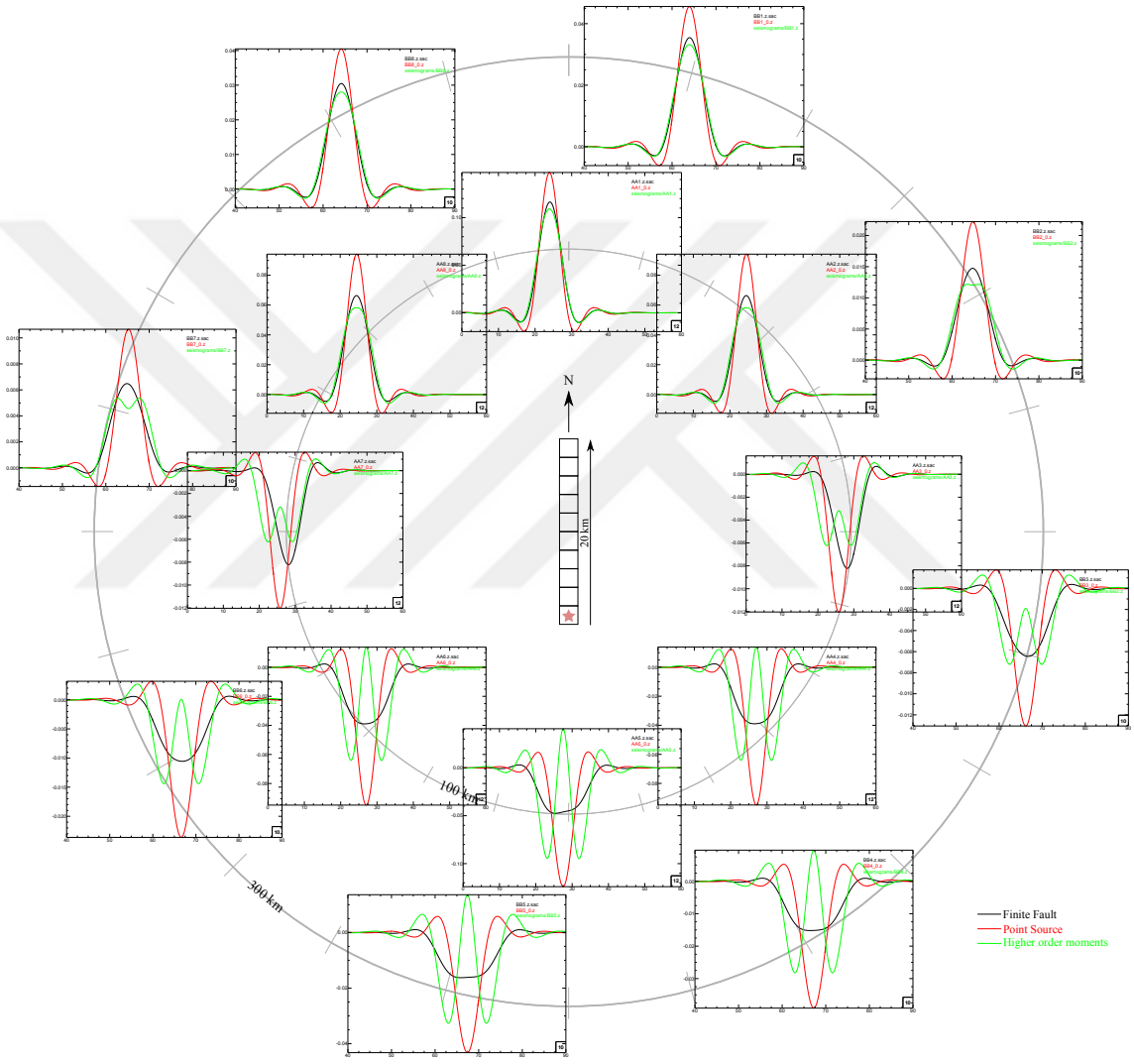

Figure 4.19. Receivers at 100 km. Azimuths start at 0 degrees and increase 45 degrees at each step (Low pass filtered $f_c = 0.1$ Hz). At the center fault model is shown. Event starts at the southmost subfault and propagates to the north.

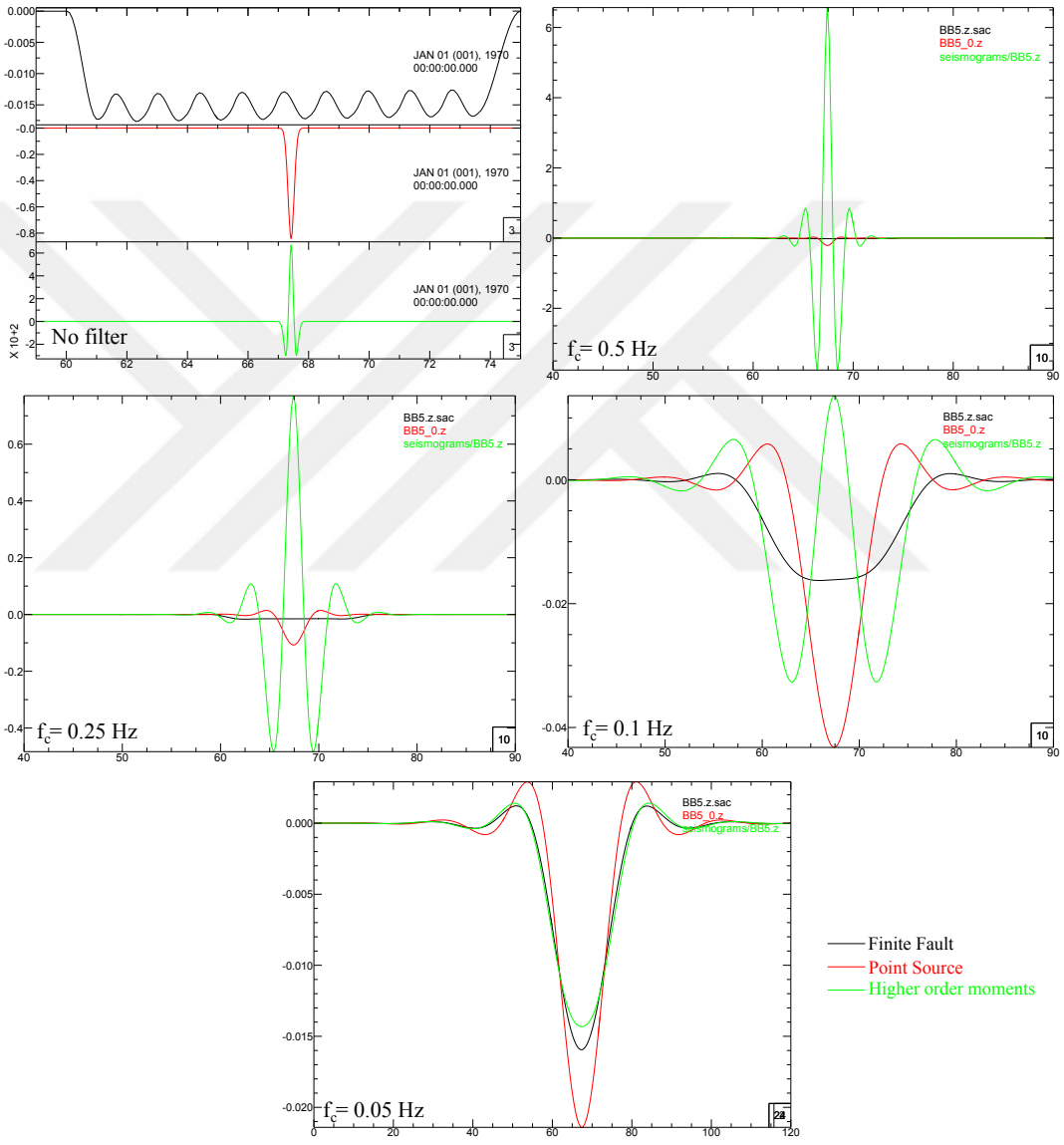

Figure 4.20. Receiver at 300 km with azimuth 190 degrees filter progression.

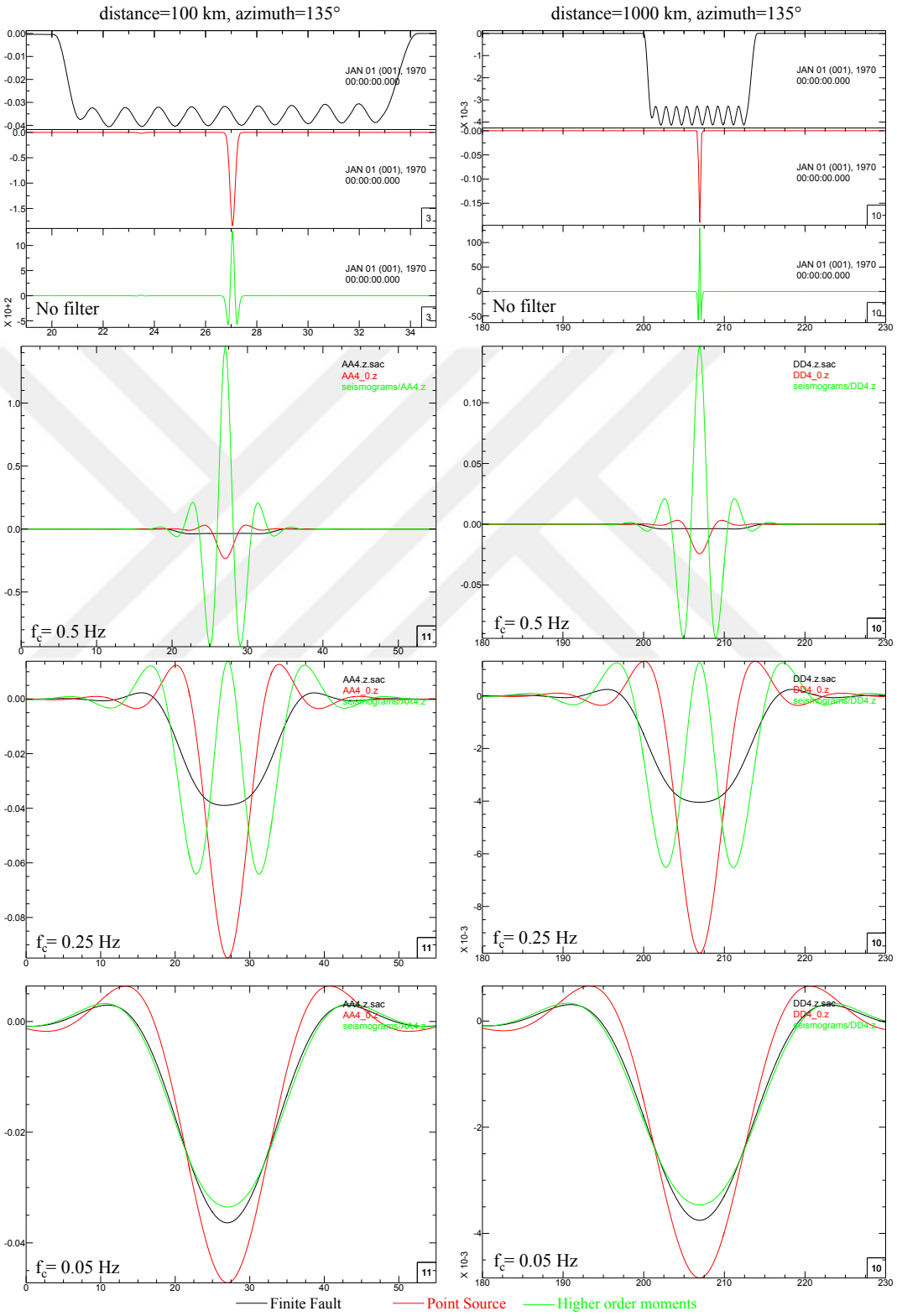

Figure 4.21. Comparisons of seismograms at different distances with the same azimuth.

4.2.3. Planar source

For this case, we use a planar finite fault model. This model has subfaults on a plane which lies in the 3D space. It has 38 subfaults along strike and 10 along down-dip. Hence, it has 380 subfaults in total. Slip distribution can be seen in Figure 4.22. Plane's strike is 270 degrees from north. Subfaults are right-lateral strike slip faults and length along strike is 2 km, length along in down-dip is 1.5 km. Rupture velocity is 3 km/s.

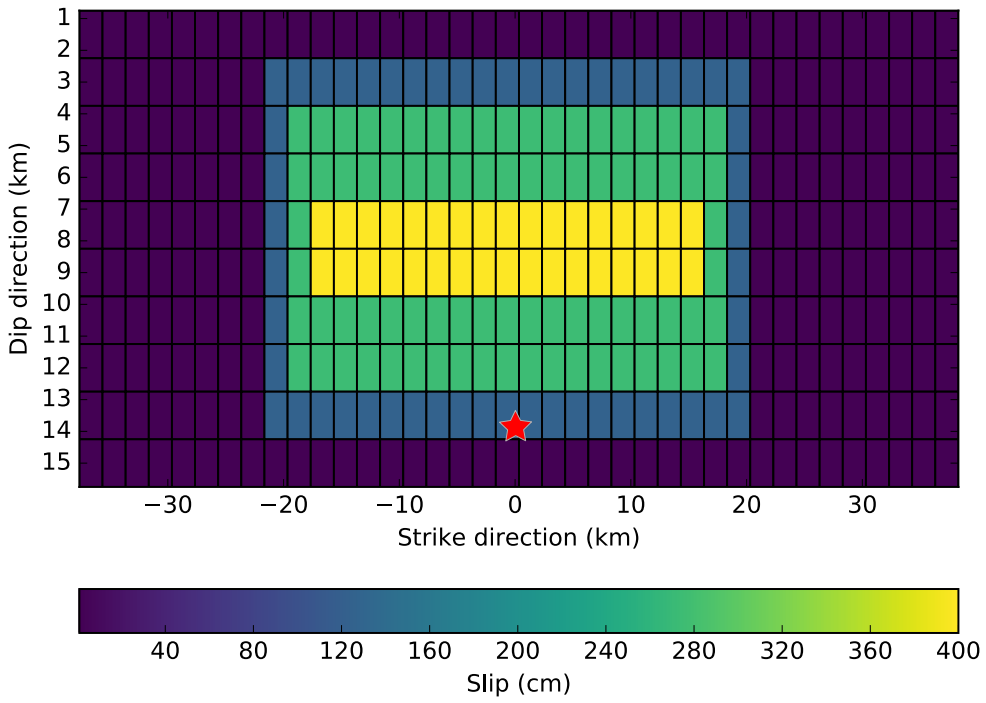

Figure 4.22. Slip distribution of fault. Hypocenter is located at (0, 14) as shown by red star.

The unfiltered seismograms at receivers located with different azimuths at a distance of 1000 km are shown in Figure 4.23.

Figure 4.24 shows the same data filtered with low-pass filter with corner frequency 0.2 Hz. Notice again that while there is no waveform similarity moment solutions and finite fault solutions in terms of shape, the pulse width similarity does exist.

When we low-pass filter the seismograms close to the corner frequency 0.1 Hz, we see similarity at 1000 km for azimuths 0, 45, 135, 225 and 315 (see Figure 4.25). For 180 they have similar Waveforms but there is a time shift. For 90 and 270 there is no similarity. But these three has lower amplitudes. 90 and 270 azimuths are also in the strike direction. This is likely to be the reason for poor performance.

In Figure 4.25, we can also observe receivers at 3000 km. Higher order moments performance is better for these receivers. The reason for that seems to be the azimuths of the receivers. Azimuths are not along the strike or exactly perpendicular (auxiliary fault direction) to it.

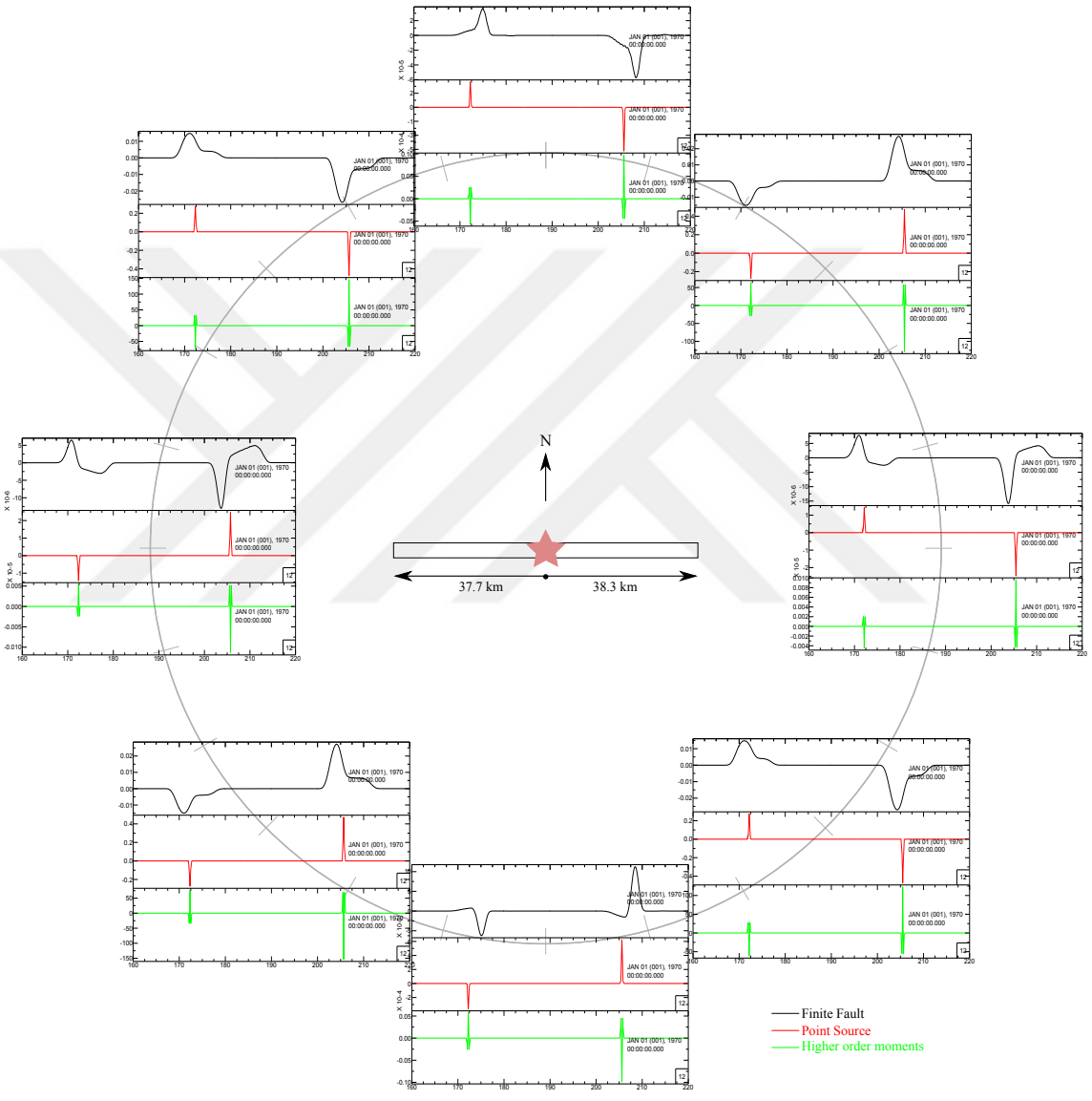

Figure 4.23. Receivers at different azimuths at 1000 km. Ticks are placed with 15 degrees interval on the circles. At the center fault model is shown. Event starts in the middle and propagates bilaterally in the west-east direction.

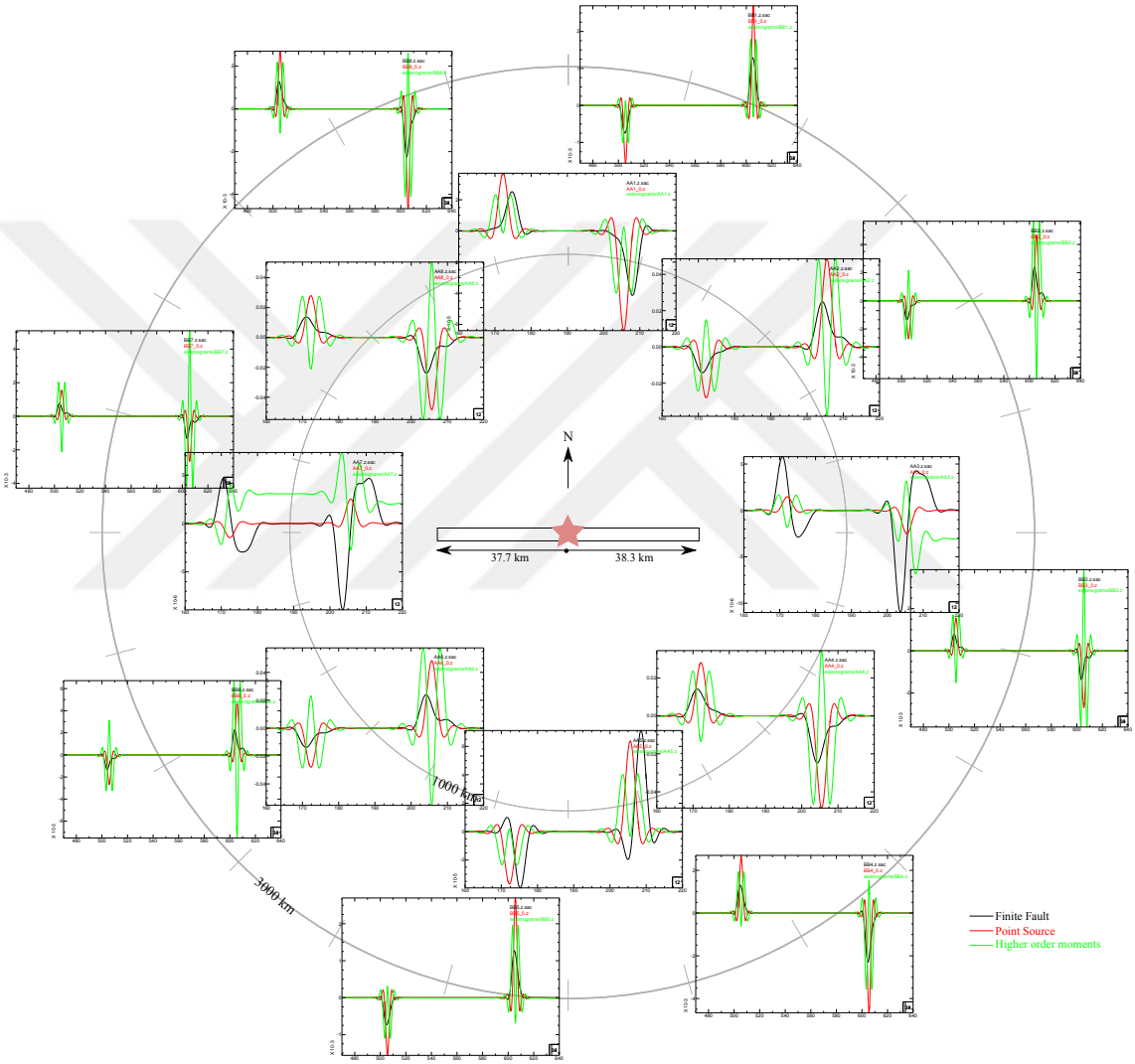

Figure 4.24. Receivers at 1000 km and 3000 km. Ticks are placed with 15 degrees interval on the circles (Low pass filtered $f_c = 0.2$ Hz). At the center fault model is shown. Event starts in the middle and propagates bilaterally in the west-east direction.

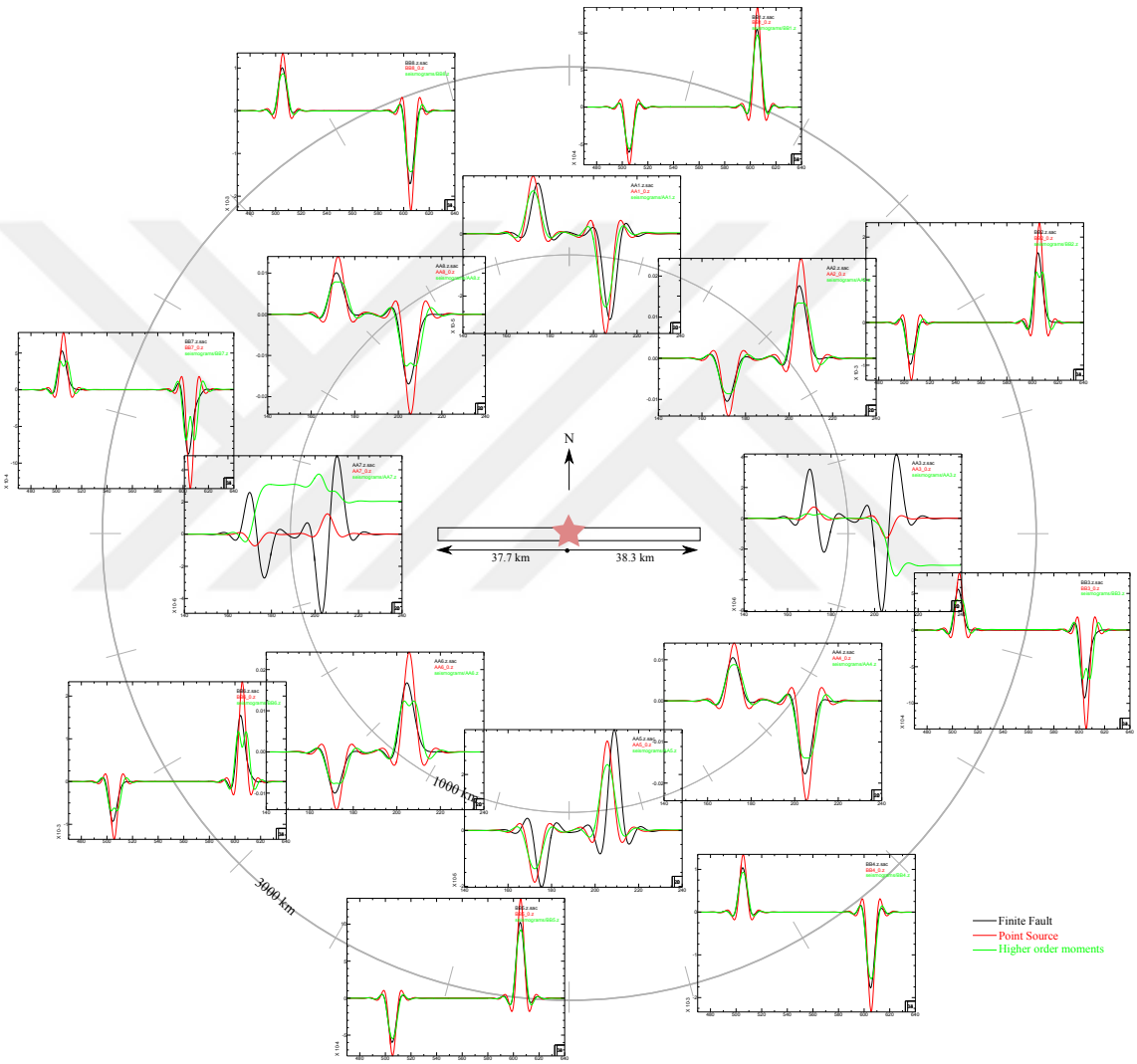

Figure 4.25. Receivers at 1000 km and 3000 km. Ticks are placed with 15 degrees interval on the circles (Low pass filtered $f_c = 0.1$ Hz). At the center fault model is shown. Event starts in the middle and propagates bilaterally in the west-east direction.

4.3. Applications Using Green's Functions for Multi-Layered Half Space

For this application we used Green's functions that are generated by frequency-wavenumber method [15]. Derivative of the Green's functions are found by finite difference method. We used the fault model in Section 4.2 for this test.

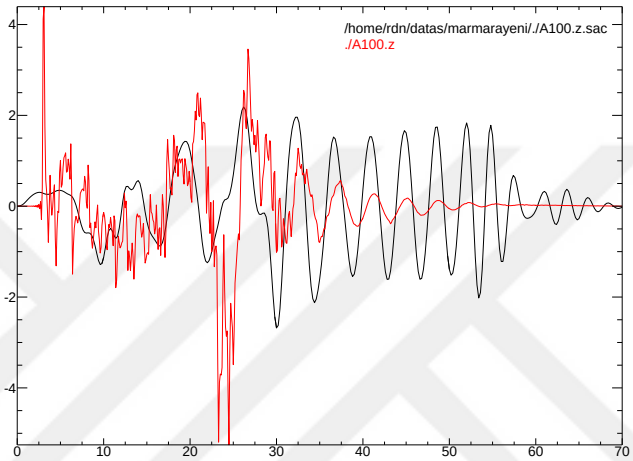

Figure 4.26. Response for a station at 100 km with 30 degrees azimuth (Black finite fault solution, Red: higher order moments solution).

Figure 4.26 shows the seismograms for a station at 100 km with 30 degrees azimuth. Seismograms for the same station with low-pass filter where the corner frequency is 0.25 Hz are shown in Figure 4.27.

For a station at 100 km with 120 degrees azimuth responses are shown in Figure 4.28. Low-pass filtered versions are shown in Figure 4.29.

It can be seen that there is some agreement between finite fault and higher order moment solution for the first station. On the other hand in the second example polarities of the first arrivals are different. This prompt us to check the derivative computations. When we tested finite difference for different point intervals. We saw that it is dependent to this variable. We tried number of methods to improve the stability of the derivatives. Appendix A talks about these methods.

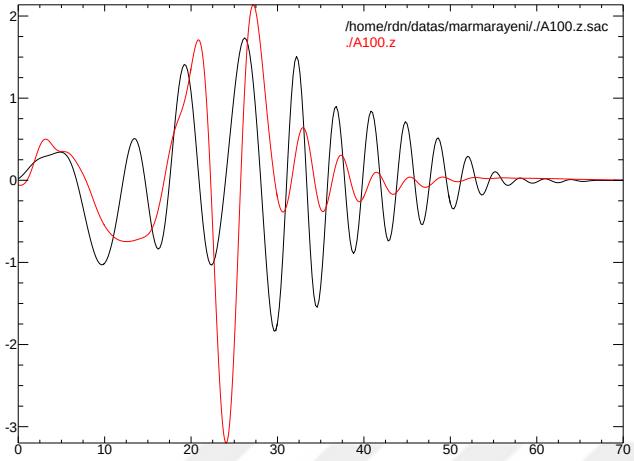

Figure 4.27. Low-pass filtered ($f_c = 0.25$) response for a station at 100 km with 30 degrees azimuth (Black: finite fault solution, Red: higher order moments solution).

We concluded that we could not produce reliable derivatives using finite difference method. We did not go further for this medium because comparisons between finite fault method and higher order moments method would not be healthy without trustworthy derivatives of the Green's functions.

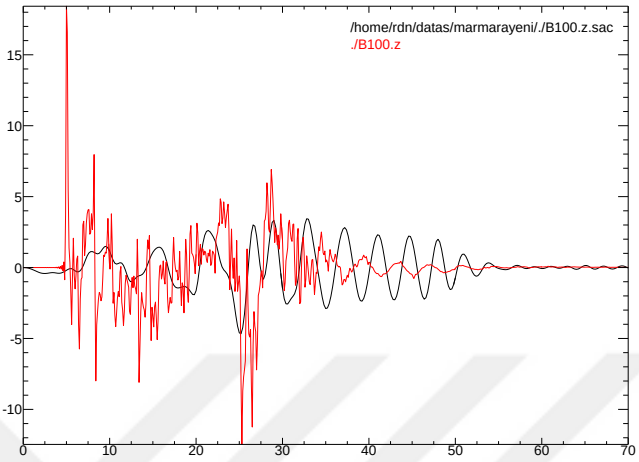

Figure 4.28. Response for a station at 100 km with azimuth 120 (Black finite fault solution, Red: higher order moments solution).

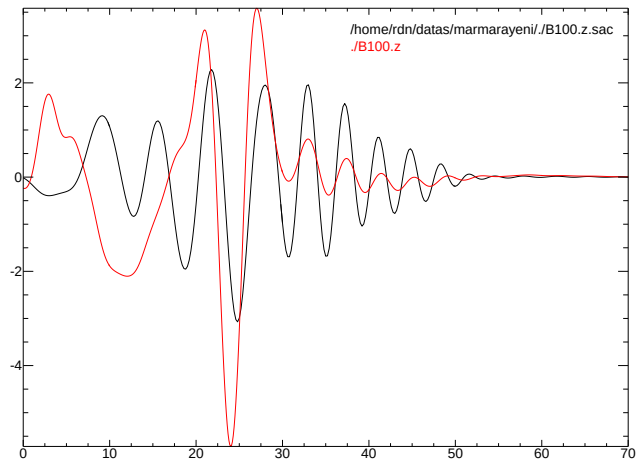

Figure 4.29. Low-pass filtered ($f_c = 0.25$) response for a station at 100 km with azimuth 120 (Black finite fault solution, Red: higher order moments solution).

5. DISCUSSION AND CONCLUSION

Main motivation for using higher order moments to represent an earthquake event is its simplicity. While finite fault method requires multiple Green's functions, higher order moments method requires only one Green's function and its derivatives. Fault model also needs to be defined a priori for finite fault modeling. Therefore, fault parameters (e.g. directivity, differentiating between auxiliary plane and fault plane) can be found more rapidly inverting for higher order moments. In this thesis, we compare the responses produced by these two methods to search for the useful parameters for inversion process.

We used the Green's function for infinite homogeneous isotropic media. This medium is selected because both Green's function and its derivatives are easy to obtain. It is found that finite faults can be approximated by its higher order moments. For infinite homogeneous isotropic media does not have any sensitivity to receiver distance. Azimuth of the receiver is more sensitive to the pulse width as expected. We conclude that fault mechanism and strike direction should be considered in selecting receivers. Receivers that are parallel to the nodal planes of the fault (fault plane or auxiliary plane) have less similarity between the finite fault solution and higher order moments solution.

The examples considered in this thesis using whole space Green's functions show that rather than direct coherence of the waveforms from finite fault sources and their higher order moment approximations, the approximations fits the broadness of the pulses better than the point source with dirac delta pulse. This reveals that if one tries to find the higher order moment parameters from the waveforms, direct comparison of waveforms is probably not the most suitable method. A modified misfit measure is needed to compare the pulse width of the real data waveforms with the higher order moment estimates. Higher order moments also improve upon the point source approximations. In the frequency ranges which faults are expected to behave like a point source, higher order moment solutions matched the finite fault solutions better than the point source responses.

We also tried to check the method for half-space layered media. Green's function generation was done by *fk* program and derivatives of Green's functions were computed using finite difference. We saw some match between finite fault and higher order moment solutions. However, we identified that derivative computation was not stable using finite difference. The results show sensitivity to grid size while taking the derivative. Therefore, we could not decide if errors between finite fault and higher order moment solutions were due to the method or finite difference derivatives, hence chose to use whole space Green's functions instead.

Although infinite homogeneous isotropic medium is a fairly simple model, it still provides valuable information about the method of higher order moments, since the higher order moments formulation does not restrict the solution to a particular medium or boundary conditions. In other words, the results for infinite homogeneous medium can be the groundwork for future studies which implement more realistic medium Green's functions. On the other hand, sensitivity for distance and azimuths could be different for different mediums and using whole-space Green's functions limits the comparison to P and S body wave waveforms. Higher order moments from surface waves are also commonly used, therefore further studies using layered media is necessary to analyze how finite-fault parameters can be obtained from surface waves.

Higher order moment calculation and seismogram generation code developed for this study is written in a way which can easily integrate another set of Green's functions and its derivatives. Therefore, one can easily implement Green's functions for more realistic media in order to further investigate the parameters that are affecting the higher order moment solutions. Further work can be done by building upon this information and perform the inversion process accordingly.

REFERENCES

1. Backus, G. and M. Mulcahy, "Moment tensors and other phenomenological descriptions of seismic sources—I. Continuous displacements", *Geophysical Journal International*, Vol. 46, No. 2, pp. 341–361, 1976.

2. Lay, T. and T. C. Wallace, *Modern global seismology*, Vol. 58, Academic press, 1995.

3. Aki, K. and P. G. Richards, *Quantitative seismology*, Vol. 1, University Science Books, 2002.

4. Konca, A. O., Y. Kaneko, N. Lapusta and J.-P. Avouac, "Kinematic inversion of physically plausible earthquake source models obtained from dynamic rupture simulations", *Bulletin of the Seismological Society of America*, Vol. 103, No. 5, pp. 2621–2644, 2013.

5. Heaton, T. H., "The 1971 San Fernando earthquake: A double event?", *Bulletin of the Seismological Society of America*, Vol. 72, No. 6A, pp. 2037–2062, 1982.

6. Backus, G. E., "Interpreting the seismic glut moments of total degree two or less", *Geophysical Journal International*, Vol. 51, No. 1, pp. 1–25, 1977.

7. Bukchin, B., "Determination of stress glut moments of total degree 2 from teleseismic surface wave amplitude spectra", *Tectonophysics*, Vol. 248, No. 3, pp. 185–191, 1995.

8. Clévédé, E., M.-P. Bouin, B. Bukchin, A. Mostinskiy and G. Patau, "New constraints on the rupture process of the 1999 August 17 Izmit earthquake deduced from estimates of stress glut rate moments", *Geophysical Journal International*, Vol. 159, No. 3, pp. 931–942, 2004.

9. Van Der Walt, S., S. C. Colbert and G. Varoquaux, "The NumPy array: a structure for efficient numerical computation", *Computing in Science & Engineering*, Vol. 13, No. 2, pp. 22–30, 2011.

10. Hunter, J. D., “Matplotlib: A 2D graphics environment”, *Computing In Science & Engineering*, Vol. 9, No. 3, pp. 90–95, 2007.

11. Beyreuther, M., R. Barsch, L. Krischer, T. Megies, Y. Behr and J. Wassermann, “ObsPy: A Python toolbox for seismology”, *Seismological Research Letters*, Vol. 81, No. 3, pp. 530–533, 2010.

12. Tapley, W. C. and J. E. Tull, “SAC-Seismic Analysis Code: Users Manual”, *Lawrence Livermore National Laboratory*, p. 388, 1992.

13. Udías, A., R. Madariaga, E. Buforn *et al.*, *Source Mechanisms of Earthquakes: Theory and Practice*, Cambridge University Press, 2014.

14. Ji, C., D. V. Helmberger, D. J. Wald and K.-F. Ma, “Slip history and dynamic implications of the 1999 Chi-Chi, Taiwan, earthquake”, *Journal of Geophysical Research: Solid Earth*, Vol. 108, No. B9, 2003.

15. Zhu, L. and L. A. Rivera, “A note on the dynamic and static displacements from a point source in multilayered media”, *Geophysical Journal International*, Vol. 148, No. 3, pp. 619–627, 2002.

16. Fornberg, B., “Generation of finite difference formulas on arbitrarily spaced grids”, *Mathematics of computation*, Vol. 51, No. 184, pp. 699–706, 1988.

17. Zhang, J.-H. and Z.-X. Yao, “Optimized explicit finite-difference schemes for spatial derivatives using maximum norm”, *Journal of Computational Physics*, Vol. 250, pp. 511–526, 2013.

APPENDIX A: TESTING FINITE DIFFERENCE STABILITY

Finite difference is a method to take derivative numerically. First forward finite difference is given in equation A.1.

$$f'(x) = \lim_{dx \to 0} \frac{f(x+dx) - f(x)}{dx} \approx \frac{f(x+dx) - f(x)}{dx} \tag{A.1}$$

It is expected that when dx gets closer to zero, result of the finite difference should approach the derivative value.

We used *fk2mt* to check the first derivatives. *fk2mt* computes the Green's function for a moment tensor using force and explosion Green's functions. We saw that finite difference can approximate the first derivative. Although, for some dx values amplitude variation can be observed. Figure A.1, shows the z derivative of z component of the Green's function. Black shows the *fk2mt* solution others are finite difference solution with dz value 0.010, 0.015 and 0.020 respectively. Finite difference solution with $dz = 0.015$ has larger amplitude than both $dz = 0.010$ and $dz = 0.020$.

It should be noted that one dx value does not work for all stations. For example, figure A.2 shows another station with the same distance as previous one but it has a different azimuth (previous one's azimuth is 90, this one's is 80). It can be seen that $dx = 0.01$ does not produce correct derivative. For this station $dx = 0.030$ gives the better result.

Instability is even more pronounced in the second derivative. Figure A.3 shows the second x derivative. You can see that middle dx value produced very different amplitude than the others. Second derivative is also hard because we have nothing to check the value with.

We tried higher order finite differences to find the stable derivative using more spatial

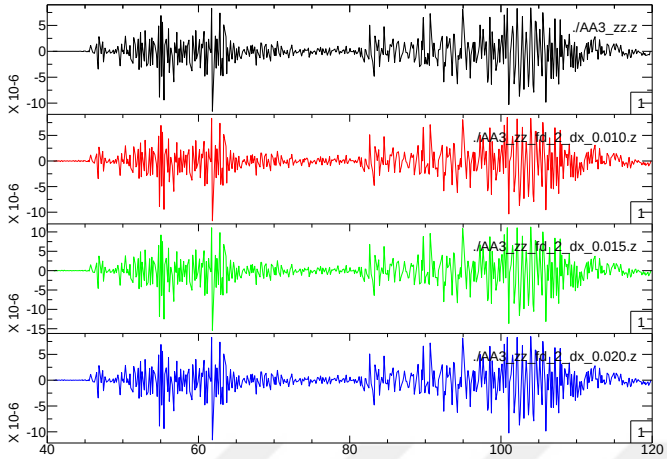

Figure A.1. First z derivative of Green's function's z component for a station at 300 km with 90 degrees azimuth (Black: *fk2mt* solution, red: finite difference with $dx = 0.01$, green: finite difference with $dx = 0.015$, blue: finite difference with $dx = 0.02$).

points [16].

In figure A.4 you can see the derivatives using 2 points. We tested 4 and 16 points finite differences to see if the results become more stable. Results can be seen in figure A.5 and A.6. These figures show us increasing number of points in the finite difference formula does not improve the result for this case.

We also tested the optimized coefficients for finite difference [17]. Result can be seen in the figure A.7. We did not see any improvements in the results.

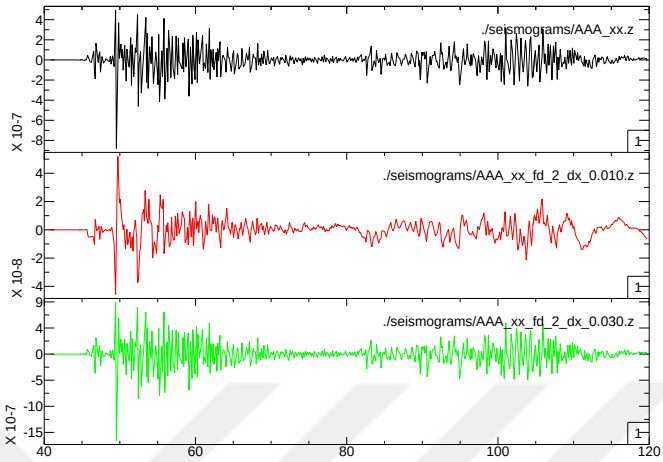

Figure A.2. First x derivative of Green's function's x component for a station at 300 km with 80 degrees azimuth (Black: *fk2mt* solution, red: finite difference with $dx = 0.01$, green: finite difference with $dx = 0.015$, blue: finite difference with $dx = 0.02$).

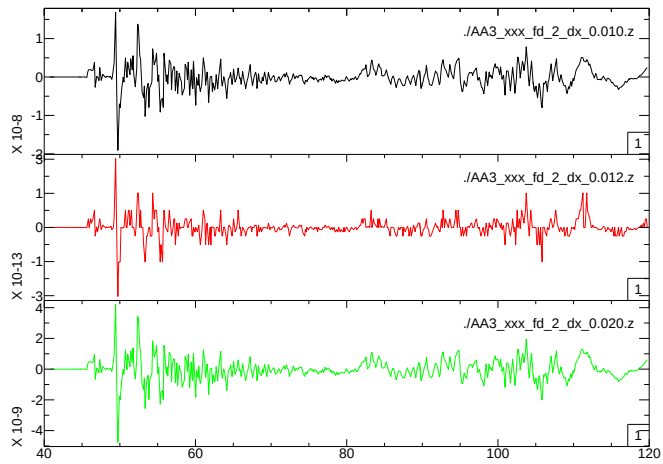

Figure A.3. Second x derivative of Green's function's x component for a station at 300 km with 80 degrees azimuth (Black: finite difference with $dx = 0.01$, red: finite difference with $dx = 0.015$, green: finite difference with $dx = 0.02$).

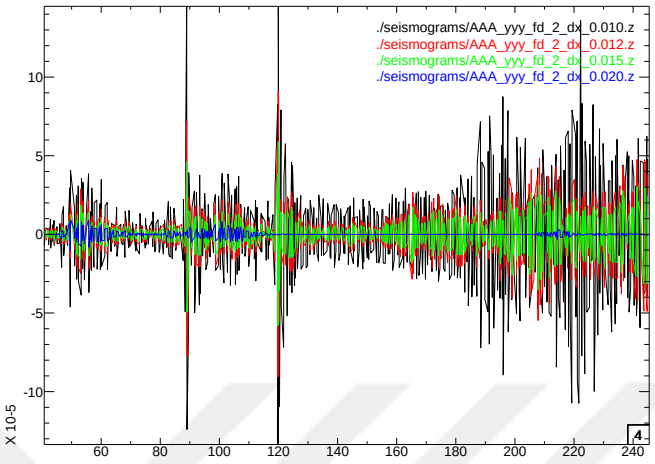

Figure A.4. Second y derivative using 2 points for a station at 300 km with 45 degrees azimuth (Black: finite difference with $dx = 0.01$, red: finite difference with $dx = 0.012$, green: finite difference with $dx = 0.015$, blue: finite difference with $dx = 0.02$).

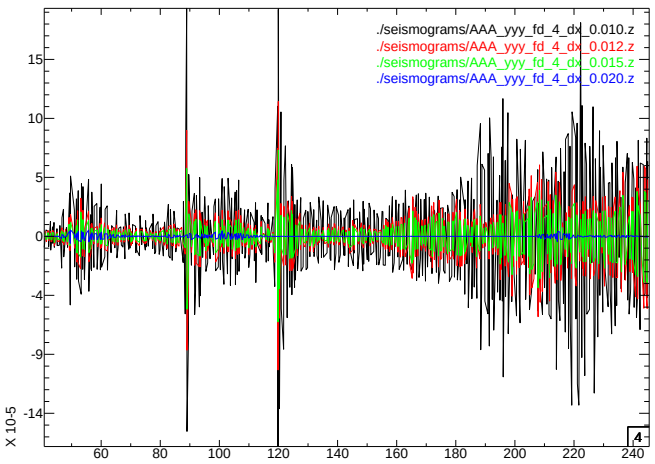

Figure A.5. Second y derivative using 4 points for a station at 300 km with 45 degrees azimuth (Black: finite difference with $dx = 0.01$, red: finite difference with $dx = 0.012$, green: finite difference with $dx = 0.015$, blue: finite difference with $dx = 0.02$).

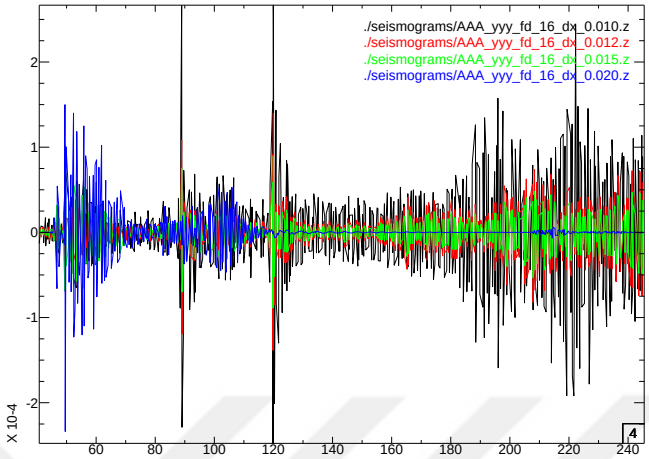

Figure A.6. Second y derivative using 16 points for a station at 300 km with 45 degrees azimuth (Black: finite difference with $dx = 0.01$, red: finite difference with $dx = 0.012$, green: finite difference with $dx = 0.015$, blue: finite difference with $dx = 0.02$).

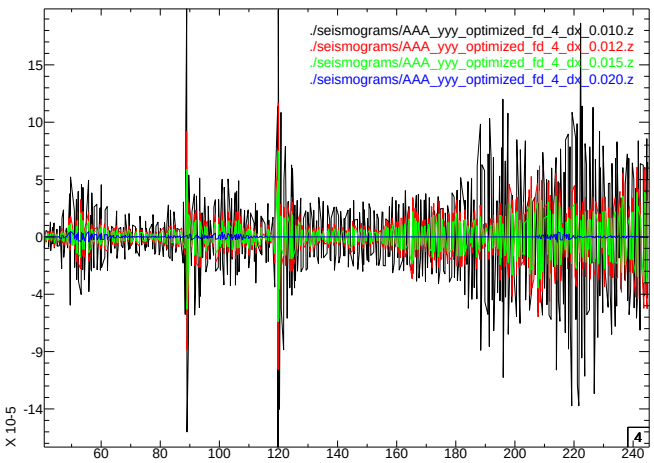

Figure A.7. Second y derivative using 4 point optimized finite difference coefficients for a station at 300 km with 45 degrees azimuth (Black: finite difference with $dx = 0.01$, red: finite difference with $dx = 0.012$, green: finite difference with $dx = 0.015$, blue: finite difference with $dx = 0.02$).